R-08-34

Impact of corrosion-derived iron on the bentonite buffer within the KBS-3H disposal concept

The Olkiluoto site as case study

Paul Wersin, Nagra

Martin Birgersson, Siv Olsson, Ola Karnland
Clay Technology

Margit Snellman, Saanio & Riekkola Oy

May 2008

Svensk Kärnbränslehantering AB
Swedish Nuclear Fuel
and Waste Management Co
Box 250, SE-101 24 Stockholm
Tel +46 8 459 84 00

ISSN 1402-3091
SKB Rapport R-08-34

Impact of corrosion-derived iron on the bentonite buffer within the KBS-3H disposal concept

The Olkiluoto site as case study

Paul Wersin, Nagra

Martin Birgersson, Siv Olsson, Ola Karnland
Clay Technology

Margit Snellman, Saanio & Riekkola Oy

May 2008

Keywords: Buffer stability, Iron-bentonite interaction, KBS-3H, Olkiluoto, Modelling.

This report is a result of a joint project between SKB and Posiva. This report is also printed as a Posiva report, Posiva 2007-11.

A pdf version of this document can be downloaded from www.skb.se.

Abstract

Steel components are unstable in EBS environments. They will corrode to fairly insoluble corrosion products, such as magnetite, and also react with the smectitic matrix of the bentonite buffer. In this study, the impact of reduced iron on the buffer's stability has been assessed within the framework of the KBS-H concept. Our work includes two parts. In the first part, available data from experimental and modelling studies have been compiled and interpreted. In the second part, a relatively simple geochemical modelling exercise on the iron-bentonite interaction in the current KBS-3H disposal system has been performed using Olkiluoto as test case. The iron in this case stems from the perforated supercontainer steel shell foreseen to be emplaced around the buffer material.

The iron-bentonite interaction under reducing conditions may involve different processes including sorption, redox and dissolution/precipitation reactions, the details of which are not yet understood. One process to consider is the sorption of corrosion-derived Fe(II). This process is fast and leads to strong binding of Fe(II) at the smectite surface. Whether this sorption reaction is accompanied by a redox and surface precipitation reaction is presently not clear. A further process to consider under very reducing conditions is the reduction of structural Fe(III) in the clay which may destabilise the montmorillonite structure. The process of greatest relevance for the buffer's performance is montmorillonite transformation in contact with reduced iron. This process is very slow and experimentally difficult to investigate. Current data suggest that the transformation process may either lead to a Fe-rich smectite (e.g. saponite) or to a non-swelling clay (berthierine or chlorite). In addition, cementation due to precipitation of iron corrosion products or of SiO_2 resulting from montmorillonite transformation may occur.

Physical properties of the buffer may in principle be affected by montmorillonite transformation or cementation processes. A preliminary study carried out by /Carlson et al. 2006/ yielded ambiguous results. The data suggested that an increase in hydraulic conductivity but no effect on swelling properties had occurred, which might be due to some cementation process. It is important to note that, at least to our knowledge, natural analogue examples displaying typical cementation features under anoxic conditions are lacking. This is contrary to examples from oxic conditions where iron oxides frequently form cementation products.

The extent of iron-bentonite interaction in a KBS-3H repository was assessed by means of (1) a mass balance estimate and (2) reactive transport modelling. The mass balance results indicated that a maximum of 10–30% of the montmorillonite in the buffer could be converted to a non-swelling Fe(II)-rich clay if all the iron from the supercontainer steel shell reacted with the clay. In the reactive transport model, site-specific geochemical data from Olkiluoto, corrosion data, Fe(II) sorption data and thermodynamic and kinetic clay data were included in a 1D diffusion model. A number of limiting test cases was run to explore the sensitivity of the results towards uncertainties in data and model assumptions. The general conclusion from the preliminary modelling study is that the extent of the zone transformed to non-swelling material is likely to remain spatially limited (a few centimetres) for very long times. Given the proximity of the physically affected area around the supercontainer steel shell to the tunnel boundary, however the potential impacts of an altered zone consisting of corrosion products and transformed clay material need to be considered in performance assessment calculations.

In order to decrease the uncertainty of the effect of the supercontainer steel shell on the buffer's stability, careful experimental studies on Fe-bentonite interaction under anoxic conditions and including measurements of physical properties should be carried out. The studies should also include diffusion experiments with Fe(II). From the modelling side, more advanced geochemical modelling (e.g. including multicomponent effects) would lead to a more realistic description of the reacting iron front.

Sammanfattning

Stålkomponenter är ostabila i ingenjörsbarriäromgivningen. De korroderar och bildar korrosionsprodukter som har låg löslighet, och reagerar också med smektitmatrisen i bentonitbufferten. I denna studie har inverkan av reducerat järn på buffertens stabilitet studerats för KBS-3H designen. I första fasen av studien sammanfattades och utvärderades tillgänglig data från experimentella och teroretiska stuider. Den andra fasen omfattade en relativit enkel geokemisk modellering av järn-bentonit växelverkan i den nuvarande KBS-3H designen baserat på platsdata från Olkiluoto. Järnet härstammar från stålhöljet av den perforerade superbehållaren som omringar bufferten och kapseln.

Växelverkan mellan järn och bentonit i reducerande förhållanden kan omfatta olika processer som sorption-, redox- och lösnings- och utfällningsreaktioner, för vilka detaljer ännu inte är kända. En process som bör noteras är sorption av Fe(II) som bildats via korrosion av järn. Denna process är relativt snabb och leder till en stark bindning av Fe(II) på smektitytan. Huruvida denna sorptionsreaktion är sammankopplad med en redox- och ytfällningsreaktion är inte klart för tillfället. En annan process som bör beaktas under mycket reducerande förhållanden är reduktion av strukturellt Fe(III) i leran vilket kan destabilisera montmorillonitstrukturen. En process av största vikt för buffertens funktion är omvandlingen av montmorillonit i kontakt med reducerat järn. Denna process är mycket långsam och svår att undersöka experimentellt. Tillgänglig data tyder på att omvandlingsrocessen kan leda till en järnrik smektit (t ex saponit) eller en icke-svällande lera (berthierine eller klorit). Ytterligare, kan cementering på grund av utfällning av järnkorrosionsprodukter aller silikat (SiO_2) äga rum som ett resultat av omvandlingen av montmorillonit.

Buffertens fysikaliska egenskaper kan i princip påverkas av omvandlingen av montmorillonit eller cementeringsprocesser. En preliminär studie som utfördes av /Carlson et al. 2006/ gav tvetydiga resultat. Resultaten pekade på en ökning i hydraulisk konduktivitet men ingen effekt på lerans svällningsegenskaper, detta kan förklaras med någon typ av cementeringsprocess. Det är viktigt att notera att vi inte känner till någon naturlig analog som skulle uppvisa ett typiskt cementeringsbeteende under syrefria förhållanden. Däremot finns det rikligt med exempel av cementeringsprodukter som bildas av järnoxider i syrerika förhållanden.

Omfattningen av inverkan av järn på bentonit i KBS-3H designen uppskattades med hjälp av (1) en massbalans beräkning och (2) en reaktiv transport modellering. Massbalansberäkningen pekade på att maximalt 10–30% av montmorilloniten i bufferten kunde omvandlas till en icke-svällande Fe(II)-rik lera om allt järn från superbehållarens stålhölje skulle reagera med leran. I den reaktiva transport modellen användes platspecifika data från Olkiluoto, korrosionsdata, Fe(II) sorptionsdata och termodynamisk och kinetisk data för leran i en 1D-diffusionsmodell. Ett antal begränsade testkörningar utfördes ör att undersöka känsligheten för osäkerheter i data modellantaganden. De generella slutsatserna från den preliminära modelleringen tyder på att omfattningen av den omvandlade zonen av bufferten till icke-svällande lermineral kommer sannolikt att förbli begränsad till ett par cm (radiellt) för en mycket lång tid. Dock med beaktande att den berörda zonen runt superbehållarens stålhölje ligger nära gränszonen till berget måste den potentiella inverkan av den förändrade zonen som består av korrosionsproukter och omvandlad montmorillonit beaktas i säkerhetsanalysen.

För att minska på osäkerheten av superbehållarens stålhöljes inverkan på buffertens stabilitet bör noggranna experimentella Fe-bentonitstudier under välkontrollerade syrefria förhållanden utföras. Dessa bör också omfatta mätningar av bufferetns fysikaliska egenskaper. Studierna bör också omfatta diffusionsstudier med Fe(II). Mera avancerade geokemiska modelleringar (t ex också beaktande av multikomponenteffekter) skulle leda till en mera realistisk beskrivning av den den reaktiva järnfronten i bufferten.

Contents

1 Introduction

Steel components are featured in most Engineered Barrier System (EBS) designs for HLW repositories. They are reactive in contact with water and will – in an anaerobic environment – corrode by producing hydrogen gas and corrosion products, such as magnetite. Moreover, the reduced iron species released from the corrosion process will react with the bentonitic material that is commonly used as buffer material. The interaction between the iron and the swelling clay might adversely affect the barrier function of the buffer and therefore should be considered in safety assessments (SA). In past safety assessments, however, this issue was usually not treated in detail. For example, in the Swiss SA *Entsorgungsnachweis,* the impact of iron from the steel canister was regarded to have a very limited effect on the bentonite buffer, owing to the low solubility of Fe(II) and preliminary experimental data /Nagra 2002/. On the other hand, recent experimental and modelling data /e.g. Wilson et al. 2006ab/ suggest that the issue of Fe-clay interaction in the EBS may need to be revisited, especially in the case of large Fe/clay mass ratios.

The KBS-3 method, based on multiple barriers, is the proposed spent fuel disposal method both in Sweden and Finland. KBS-3H and KBS-3V are the two design alternatives of the KBS-3 spent fuel disposal method. Posiva and SKB have conducted a joint research, demonstration and development (RD&D) programme in 2002–2007 with the overall aim of establishing whether KBS-3H represents a feasible alternative to KBS-3V. Within the KBS-3H concept, a large mass of carbon steel in the EBS system is foreseen. In this concept, prefabricated modules of copper canisters containing spent fuel, surrounded by Na-rich bentonite (MX-80) blocks and an outer thin perforated steel supercontainer (SC), are emplaced in horizontal tunnels (Figure 1-1). A distance block of bentonite is positioned between the SCs to provide sufficient minimum spacing between SCs for thermal reasons and to isolate SCs hydraulically during saturation. Upon tunnel closure, groundwater from the granitic host rock will saturate the buffer material, which will swell and extrude through the holes in the SC, resulting in an effective seal around the canisters. On the other hand, corrosion processes will occur, leading to the production of significant quantities of oxidized iron species and hydrogen.

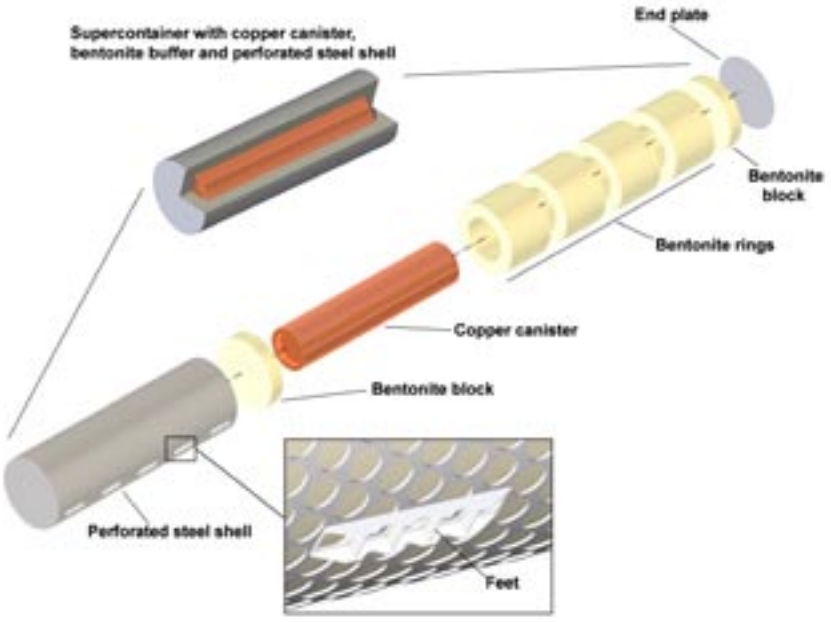

Figure 1-1. *Exploded view of the KBS-3H supercontainer with buffer and copper canister.*

The scope of this study is to assess the impact of iron components released from the corrosion process on the bentonite buffer within the KBS-3H concept, using the Olkiluoto site in Finland as a test case. The adopted procedure is (1) to compile available experimental and natural analogue data from the literature and to identify and evaluate the relevant processes, (2) to analyze geochemical site-specific data from the Olkiluoto site and (3) to perform a bounding analysis on detrimental effects of Fe on the swelling fraction by applying geochemical modelling.
A preliminary modelling exercise on this issue was performed previously /Johnson et al. 2005/. This study updates and extends this first quantitative analysis.

2 Fe – smectite interaction: literature review

2.1 Corrosion aspects

2.1.1 Initial oxidizing conditions in the EBS

Zero-valent iron is unstable in water and corrodes by forming an oxide-type surface layer. The corrosion of carbon steel under aerated conditions in the initial aerobic stage after repository closure is relatively rapid. The relatively short aerobic stage after repository closure is indicated from simple bounding calculations. For example, /Wersin et al. 1994/ calculated timescales for the vertical KBS-3 design on the basis of the reaction of O_2 with pyrite in the bentonite to range from 7 to 290 years. This estimate used a conservative pyrite oxidation model (shrinking core model) and neglected the O_2 migration and reaction in the host rock. In fact, microbially-mediated and/or inorganic reactions in the granitic host rock are expected to accelerate O_2 consumption rates, as was shown in the REX experiment at Äspö /Puigdomenech et al. 2001/ and by a recent experimental study /Rivas Perez et al. 2005/. From these considerations, the timescale for O_2 depletion is likely to be a few years to a few decades.

In the case of KBS-3H, it might seem at first sight that SC corrosion traps most of the residual near field (NF) oxygen. However, considering that during the initial stage the heat from the canister will move the water front towards the outer side of the buffer, the cathodic reaction may be limited by slow diffusion, especially in case of low hydraulic conductivity of the host rock. Calculations performed for the Swiss design concept (initial bentonite dry density = 1.5 Mg/m^3; initial moisture content = 2%) under the assumption that O_2 is consumed entirely by steel corrosion at fully saturated conditions indicate timescales for oxygen depletion of about 20–50 years /Wersin et al. 2003/. This estimate is based on the assumption that O_2 depletion occurs entirely by inorganic reaction processes. For the KBS-3H drift, saturation times of the buffer will vary because of variable hydraulic conditions in different sections and this may also affect oxygen consumption rates. Although it is likely that oxygen in the gap between the supercontainer steel shell and the rock will be consumed rapidly (within months to years) by microbially-induced reactions and SC corrosion, the oxygen trapped inside the buffer will be depleted more slowly. In the outer part of the buffer, if this is near saturation, the rate of depletion will be controlled by the slow rate at which oxygen will migrate by aqueous diffusion to the outer surface, where again it will be consumed by relatively rapid microbially-induced reactions and by steel corrosion. In the inner part of the buffer, if unsaturated, oxygen will be transported relatively rapidly to the copper canister surface, but reaction with copper will be slow. Much of this oxygen may again therefore, ultimately be consumed by microbially-induced reactions and by steel corrosion at the outer boundary of the buffer. Since the presence of the steel supercontainer and other steel components in the KBS-3H concept provides an additional sink for oxygen depletion, in addition to those discussed above (valid for KBS-3V), the timescale for oxygen depletion will certainly be no longer than that in KBS-3V (a few years to, pessimistically, a few hundred years), but could be somewhat less /Smith et al. 2007/.

Recent results from the large-scale tests on oxygen consumption in bentonite in the framework of the LOT project showed that, although the mechanism is not clear, oxygen initially present in bentonite is completely consumed within a few years /Muurinen 2006/ From these considerations, timescales of oxygen depletion will be short, at maximum a few decades, regardless of whether additional steel components, such as in the KBS-3H, are emplaced or not.

2.1.2 Corrosion rates and corrosion products under anaerobic conditions

Under anoxic conditions iron corrodes by the reaction with water according to the overall reaction:

$$3Fe + 4H_2O \rightarrow Fe_3O_4 + 4H_2 \qquad \text{(Equation 2-1)}$$

The reaction is shown for the corrosion reaction to magnetite, which is the corrosion product observed in the great majority of the experiments relevant to repository conditions. The formation of the protective oxide layer leads to a strong decrease in corrosion rate. This is shown by a number of corrosion experiments for carbon steel under a variety of solution conditions in which a significant decrease of the corrosion rates with time is noted. Thus, corrosion rates determined from weight loss and hydrogen production measurements show a decrease from 20 µm a^{-1} to less than 5 µm a^{-1}. This is illustrated in Figure 2-1 taken from a compilation of /Andra 2001/. The results suggest that the nature of anions (chloride, carbonate, sulphate) does not significantly affect corrosion rates under anoxic conditions.

Recent corrosion experiments in different artificial groundwaters performed by /Smart et al. 2001/ within SKB's research program showed that anaerobic corrosion rates declined from the initial values of 10–30 µm a^{-1} to low values of 0.1 µm a^{-1} upon growth of a protective magnetite layer. The long-term rates showed no significant influence of temperature within the range of 30–85°C. Later experiments performed in compacted bentonite /Smart et al. 2004/ revealed higher rates compared to those obtained in water media. The corrosion rates obtained for a period of about 1 year were 1–2 µm a^{-1}. The higher long-term rate was explained by slower build up of the protective magnetite film because of incorporation of released iron in the clay. On the other hand, /Xia et al. 2005/, who also performed corrosion studies in compacted bentonite, deduced low corrosion rates of 0.1 µm over a corrosion period of 5 months, while identifying a rather significant iron reaction front.

Since experimental studies can assess only a limited time frame, natural and archaeological analogues data can yield valuable information. A comprehensive review on archaeological analogues and corrosion by /David 2001/ demonstrates that the majority of iron objects experienced corrosion of 0.1–10 µm a^{-1}. This suggests low and relatively uniform long-term corrosion rates in very different geochemical environments.

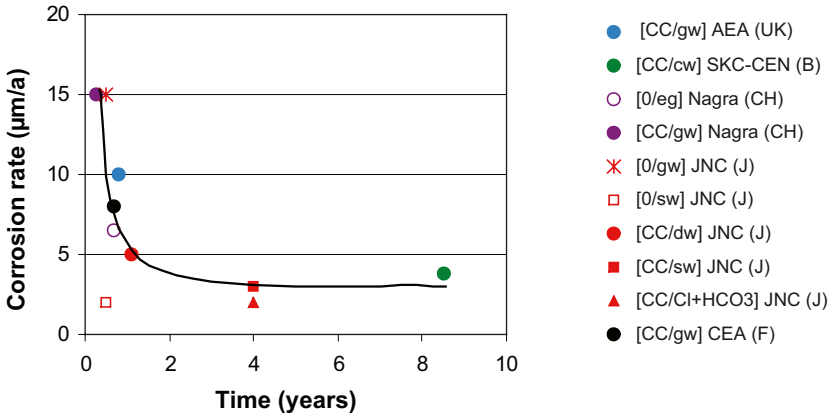

Figure 2-1. *Compilation of experimentally determined anoxic corrosion rates (modified from /Andra 2001/), CC: compacted clay; 0: immersion, gw: granite water; cw: clay water, sw: sea water, dw: distilled water.*

Pitting

Pitting and crevice corrosion are favoured when the cathodic and anodic reaction are physically separated, which in turn results from heterogeneities within the material or gradients within the solution. For example, attack of the passivating oxide layer by chloride or sulphate leads to localised corrosion under oxic conditions.

The effect of pitting decreases with corrosion depth. This is evident from a compilation of pitting factors taken from laboratory studies and iron samples buried in soils for periods up to 15 years /JNC 2000/. This shows that pitting factors strongly decrease with corrosion depth. At a corrosion depth of 1 mm, the maximum pitting factors drop below 5 /Johnson and King 2003/.

Anaerobic corrosion of steel is much more uniform than that under aerated conditions and pitting factors are very low. Some pitting may occur in the presence of sulphide and/or the presence of microbes (see sections below).

Nature of corrosion products

The dominant anaerobic corrosion product that is experimentally observed under near-neutral and alkaline conditions is magnetite. It forms a very stable and insoluble phase. The stability of magnetite increases with increasing temperature /Hermansson 2004/. Results obtained from /Smart et al. 2001/ indicate that magnetite occurs as a thin (< 100 nm) uniform inner layer and a porous outer layer.

Depending on solution conditions other Fe corrosion products may also form. Thus, at high concentrations of sulphide or carbonate, iron sulphide or siderite precipitation is expected:

$$Fe + HS^- + H^+ \rightarrow FeS + H_2 \qquad \text{(Equation 2-2)}$$

$$Fe + HCO_3^- + H^+ \rightarrow FeCO_3 + H_2 \qquad \text{(Equation 2-3)}$$

In addition, green rust type phases (layered double Fe(III)/Fe(II) hydroxides) may form, which are expected to be metastable under conditions of interest with respect to magnetite and siderite /Génin et al. 1998/.

The stability field of the different possible iron corrosion products can be presented in classical Eh-pH diagrams. Figure 2-2 illustrates two such diagrams constructed for conditions representative of deep groundwaters at Olkiluoto (cf. Chapter 3). As shown therein, magnetite is the stable Fe phase at pH values higher than 8. FeS (Figure 2-2a) is also thermodynamically stable under conditions expected for the repository. On the other hand, pyrite (not shown here) has a much larger stability field; its formation however may be limited by slow kinetics. An indication that pyrite formation may not be relevant under repository conditions stems from the observed groundwater composition in the host rock, which indicate equilibrium with FeS rather than with FeS_2 (Section 3.2). Siderite formation is in principle also possible (Figure 2-2b) but requires high carbonate and low sulphide activities in the groundwater. As discussed in /Johnson et al. 2005/, the amount of siderite formed is expected to be less than that of magnetite because of slow carbonate flux relative to the corrosion rate.

Observations from archaeological objects buried in sediments /David 2001/ showed the presence of magnetite and iron sulphides and to a lesser extent of siderite, on iron surfaces.

In addition to hydroxide, sulphide and carbonate, corrosion-released Fe(II) may react with dissolved silicate and the solid clay fraction. This reaction can be schematically written as:

$$Fe + H_4SiO_4 \rightarrow FeSiO_3 + H_2 + H_2O \qquad \text{(Equation 2-4)}$$

Little is known about the details of this process, such as the nature of the iron silicate phases and the thermodynamic and kinetic constraints. This aspect is discussed in detail in Section 2.3.

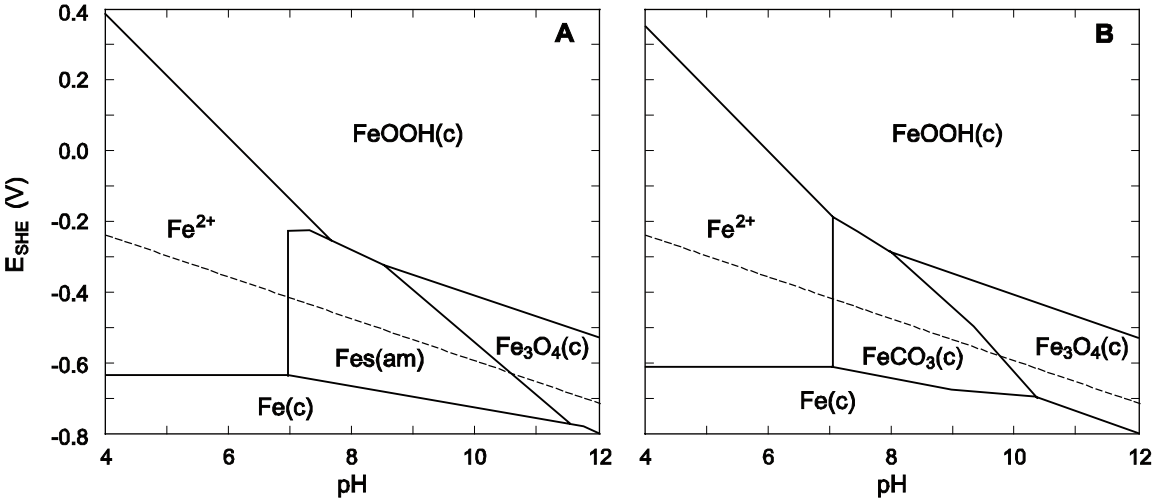

Figure 2-2. *pH-Eh diagram showing stability fields of potential corrosion products for conditions representative of the Olkiluoto site (pH 7.5–8, Eh –300 to –200 mV); left: conditions representing sulphate reduction zone (Fe = 1e–5 M, HS_{tot} = 1e–5 M, DIC = 5e–4 M); right: iron reduction zone with low sulphide (Fe = 5e–5 M, HS_{tot} = 1e–6 M, DIC = 5e–3 M).*

Effect of microbial activity

Compacted bentonite acts as an efficient filter towards microbes. As shown by /Pusch 1999/, sulphate-reducing bacteria (SRB) are immobile in bentonite exceeding 1.9 Mg m^{-3} saturated density. Moreover, experiments performed by Pedersen and co-workers /e.g. Pedersen 2000/ showed that the activity of SRB in bentonite ceases at dry densities higher than 1.5 Mg m^{-3}. Based on past and ongoing studies /e.g. Stroes-Gascoyne et al. 2006/, a swelling pressure criteria of > 2 MPa for the buffer has recently been defined by SKB /SKB 2006a/ in order to prevent bacterial activity. This swelling pressure corresponds to a buffer density of 1.8 Mg m^{-3} /SKB 2006b/. Studies performed by /JNC 2000/ confirmed that SRB introduced into 70/30 bentonite/sand mixtures at a dry density of 1.6 Mg m^{-3} (and thus a significantly lower effective clay density) surrounding steel samples had no effect on corrosion rates and were not cultivatable after the test. As a consequence, it is not expected that microbially-mediated sulphate reduction will occur in compacted bentonite.

On the other hand, the situation may be different for the outermost part of the bentonite buffer and for the SC in the KBS-3H concept. Due to the short distance to the host rock, the lower density of the clay extruded through the holes in the SC and the possibility of transformation of the clay matrix between the SC and the host rock (see Section 2.5), microbes might be viable and reach and attach to the SC surfaces.

Microbial activity is known to influence iron corrosion. For example, the presence of SRB on the surface of steel may lead to increased attack by sulphide and thus affect the formation of the protective oxide layer. Moreover, iron-reducing bacteria (IRB) might be active by adhering to the magnetite layer and promoting reductive dissolution of the Fe(III) component /Kostka and Nealson 1995, Dong et al. 2000/. In addition, the possibility of autotrophic methanogenic bacteria promoting degradation of inorganic carbon by using the hydrogen source could be relevant. These three bacterially-mediated processes are probably occurring within the deep groundwaters at Olkiluoto (see Section 3.2.1). Hence, in principle, it is conceivable that they may also occur in the SC environment.

The microbial effects on corrosion rates are not expected to be very large, based on observations of archaeological analogues. If, for example, SRB were active at the SC surface, this would favour a sulphide precipitation layer, which would also be protective against high corrosion. However, in this case increased pitting may occur /Johnson and King 2003/. Similarly, the build up of Fe^{2+} by IRB on magnetite-coated steel is limited by sulphide and siderite precipitation as

well as by the slow dissolution kinetics /Dong et al. 2000/. The impact of thriving methanogenic bacteria on corrosion is uncertain. Consumption of H_2 would occur and this might slow down the pressure build up of hydrogen gas. Reduction of inorganic carbon would limit siderite precipitation and, in the case of simultaneous sulphate reduction, counteract alkalinity increase.

2.2 Sorption and redox processes

2.2.1 Sorption of Fe^{2+}

Iron released from the corrosion process will not only precipitate as separate corrosion products, but may also interact with the clay matrix via sorption. Under reducing conditions, sorption processes involving Fe(II) will be predominant. So far, there has been little work on this topic, a notable exception being the recent studies of Charlet and co-workers within Andra's R&D program /Andra 2005, Tournassat 2003, Charlet and Tournassat 2005/. The outcome thereof can be summarized as follows:

Under reducing conditions, sorption of Fe^{2+} to montmorillonite occurs like other metal cations such as Ni(II) or Zn(II) /e.g. Bradbury and Baeyens 1997/: i.e. by cation exchange in the interlayer and surface complexation to edge sites. The sorption data could be adequately modelled with an ion exchange/surface complexation model. In general, sorption of Fe^{2+} was shown to be extremely strong, above pH values of 4. At low pH, Fe^{2+} was shown to sorb via cation exchange with a selectivity coefficient very similar to that of Ca^{2+}. At pH values between 4 and 7, surface complexation to edge sites was the dominant sorption process. At pH values above 7.0, the interaction process became more complex and both oxidation of Fe^{2+} and surface precipitation of a Fe(II) silicate phase were noted. However, all data could be reasonably well modelled using a cation exchange/surface complexation approach. It was postulated that oxidation of Fe^{2+} to Fe^{3+} at higher pH was not caused by molecular O_2 because care had been taken to avoid O_2 contamination and because desorption data indicated reversibility. The authors advanced the hypotheses that Fe^{2+} oxidation results from interaction with structural Fe(III) or by reduction of water. Oxidation of sorbed Fe^{2+} under anoxic conditions has also been reported in earlier work /Gerstl and Banin 1980/.

Because of the very high specific sorption of Fe(II) to the clay, the question arises about the competition effect towards radionuclides. Preliminary data with Eu(III) presented by /Charlet 2006/ suggest an enhancing sorption effect rather than competition. However, clearly more sorption data are needed to clarify this point.

2.2.2 Reduction of structural Fe^{3+}

There is abundant literature on the reduction of structural Fe^{3+} in smectites. Most of the recent experimental work has been performed within the research group of Dr. Stucki who investigated the reduction of smectite with dithionite /e.g. Stucki et al. 1984ab, 2000/ and with bacteria /Kostka et al. 1996, 1999/. The Fe^{3+} reduction resulted in an increase in layer charge, a decrease in swelling pressure (but see comments on this work given in Section 2.4) and decrease in particle surface area. As indicated from the study of /Lantenois 2003/ and interpreted by /Lanson 2006/, iron powder in contact with diochtahedral smectite may also induce reduction of octahedral Fe(III) (see following section).

The charge deficit resulting from Fe^{3+} reduction has been shown to be compensated by adsorption of an exchangeable cation and/or dehydroxylation of structural OH^-. The detailed mechanism, however, is still controversial /e.g. Heller-Kallai 1997, Drits and Manceau 2000/. For example, /Lanson 2006/ proposed for the interaction of Fe(0) with smectite an initial deprotonation of structural OH followed by Fe(0) oxidation and migration of released Fe(II) to the clay surface and in the interlayer, which would subsequently trigger Fe(III) reduction via electron transfer. Further, this author and also /Drits and Manceau 2000/ propose that the reduction process in turn leads to lattice destabilisation and migration of Fe^{2+} to vacant sites to form high-energy domains, thus further destabilising the crystal structure.

/Shen et al. 1992/ studied the effect of iron reduction in nontronite and montmorillonite on hydraulic conductivity by using sodium dithionite as reducing agent. The results indicated a significant increase in hydraulic conductivity for both minerals upon reduction of structural Fe^{3+}. However, we have reason to question the conclusions made in this work as further discussed in Section 2.4.

2.3 Mineral transformation processes

Contrary to sorption, the mineral transformation processes involving smectite and Fe will be slow and driven by kinetics /e.g. Andra 2005/. This is indicated from available experimental data (see Section 2.3.2). Unfortunately, due to the lack of consistent data, the nature of reaction products relevant to repository conditions as well as transformation rates and reaction pathways are poorly known. It is useful to first briefly visit the mineralogy of Fe bearing clays and their respective geochemical environments where they are encountered.

2.3.1 Fe-bearing clays

Iron, as Fe^{3+} and Fe^{2+}, is one of the principal elements present in the clay lattice. Fe^{3+} generally substitutes for Al in dioctahedral positions, whereas Fe^{2+} replaces Mg^{2+} in trioctahedral positions. The replacement of Al^{3+} by Fe^{3+} in tetrahedral positions is far less frequent. The Fe^{3+}/Fe^{2+} ratio is representative of redox conditions during the formation of the clay.

In the 1:1 clays (kaolinite/serpentine group), the most common iron-rich minerals are:

- **Greenalite** $(Fe^{2+}, Fe^{3+})_{2-3}Si_2O_5(OH)_4$: Iron occurs mainly as Fe^{2+} in trioctahedral position. A typical simplified formula is $Fe_3^{2+}Si_2O_5(OH)_4$. Greenalite is not very common and generally found in low grade metamorphic rocks. It is frequently associated with stilpnomelane, chamosite, magnetite, siderite, quartz, and minnesotaite (a 1:1 clay similar to greenalite).
- **Berthierine** $(Fe^{2+}, Fe^{3+}, Al, Mg)_{2-3}(Si, Al)_2O_5(OH)_4$: Iron occurs mainly as Fe^{2+} in trioctahedral position. Substitutions of Fe^{2+} by Fe^{3+} are predominantly compensated by the tetrahedral charge deficit related to Al^{3+}-Si^{4+} substitutions. Berthierine is the most common of the iron-rich 1:1 clays. For the Fe-rich end member, a simplified formula is $(Fe_2^{2+}Al)(SiAl)O_5(OH)_4$ /Meunier 2005/. It is formed in un-metamorphosed marine sediments and lateritic and polar soils. Berthierine is one of the precursor minerals of chlorite in clastic sediments. Its formation is favoured in anoxic iron-rich and K-poor environments relative to glauconite /Berner 1980/. The transition of berthierine to chlorite during diagenesis occurs between temperatures of 65 and 130°C according to /Iijima and Matsumoto 1982/, which is in agreement with observations in sediments of the North Sea /Aagard et al. 2000/. Berthierine and chamosite often form mixed layers, which have shown experimentally to be transformed to chlorite at 200–250°C /Aagard et al. 2000/.
- **Odinite** $(Fe^{3+}, Mg, Al, Fe^{2+})_{2.5}(Si, Al)_2O_5(OH)_4$: Iron occurs mainly as Fe^{3+} in dioctahedral position. The trioctahedral position is occupied mainly by Mg^{2+}. Odinite is formed in marine waters and shallow sediments. It is also a common precursor for chlorite formation.
- **Cronstedtite** $(Fe^{2+}, Fe^{3+})(Si, Fe^{3+})O_5(OH)_4$: This trioctahedral mineral is the most iron-rich of this mineral family. One out of three Fe^{2+} is substituted by Fe^{3+}. It frequently occurs as an alteration product of iron-rich meteorites and in low temperature hydrothermal sulphide rocks.

The 2:1 clays have a variety of Fe-bearing minerals and mineral groups. In **smectites**, iron is far less abundant than in 1:1 structures. In the dioctahedral smectites, Fe^{3+} is the predominant oxidation state (replacing Al^{3+} mainly in octahedral position) whereas in the trioctahedral series Fe^{2+} is the predominant oxidation state. Because of steric hindrance and the larger size of Fe^{3+} relative to Al^{3+} in the octahedral cavity, montmorillonites normally contain little iron. Trioactahedral smectites are the most Fe^{2+}-rich smectite members. The most common Fe-rich smectite minerals are:

- **Nontronite,** with the formula $(Ca_{0.5}, Na)_{0.3}(Fe^{3+})_2(Si, Al)_4O_{10}(OH)_2$, a smectite, whose negative charge is induced by tetrahedral substitution of Al^{3+} for Si^{4+}. The main oxidation state is Fe^{3+}. Nontronites are formed by weathering of sediments or alkaline volcanic rocks under intermediate redox conditions in low temperature or hydrothermal environments. In the latter case, they are frequently associated with saponites and celadonites /Buatier et al. 1989/. The structural Fe^{3+} in nontronites can be reduced by strong reductants or bacteria, leading to an increase in layer charge to compensate the charge deficit (see Section 2.2.2).
- **Saponite**, a trioctahedral smectite, in its iron-rich variety can be expressed as $(Ca_{0.5}, Na)_x(Fe^{2+}, Mg)_3(Si_{4-x}, Al_x)O_{10}(OH)_2$. Saponites contain substantially larger amounts of Fe^{2+} than dioctahedral smectite. They are encountered in hydrothermal reducing environments and can form at rather high temperatures of 150–200°C /Badaut et al. 1985/. They are also found in marine sediments as alteration products from volcanic glass in reducing environments /Güven 1988/. Stevensite, another trioctahedral iron-rich smectite is less frequent than saponite, but is often found in association with the latter.

Another group in the 2:1 series, the **micas**, has the following iron-rich varieties:

- **Glauconite,** $K_2(Fe^{3+}, Al, Fe^{2+}, Mg)_4Si_{8-x}, Al_xO_{20}(OH)_4$ occurs predominantly in marine sediments (sandstones and limestones) and is formed in shallow marine environments under intermediate redox conditions. Although Fe^{3+} is the main oxidation state, glauconites are sometimes found to be associated with pyrite at rather low Eh conditions and high Si activities, whereas at low Si activities berthierine is formed /Meunier 2005/.
- **Celadonite** $K_2(Fe^{3+}, Al)_2(Fe^{2+}, Mg)_2Si_8O_{20}(OH)_4$ is encountered in a various geological settings and is formed under conditions rich in Fe ad K over a large range of temperatures (from ambient up to 180°C) /Gallahan and Duncan 1994, Cathelineau and Izquierdo 1988/.

The final mineral group in the 2:1 layer series are the **chlorites**. These are the most abundant Fe-rich clay minerals. They have a wide compositional range and can form a variety of solid solutions, also between dioctahedral and trioctahedral poles, although being predominantly of trioctahedral nature. Chlorites are generally formed at higher temperatures than other clay minerals; usually above 150°C. Precursor minerals for chlorite are smectites, vermiculite and berthierine. In diagenetic sediments, there exists a progressive series of smectite/chlorite mixed layers. Under hydrothermal conditions, on the other hand, chlorite and smectite precipitate as separate mineral phases /Meunier 2005/.

- **Chamosite** with the typical formula $(Fe, Mg)_5Al(Si_3Al)O_{10}(OH)_8$ is the most iron-rich member, where Fe^{2+} is the predominant oxidation state. As noted above, it may form mixed layers with berthierine and also replace this mineral with increases in temperature.

2.3.2 Experimental data on smectite-Fe interactions

Relevant experimental data, namely on the interaction of Fe^0 or Fe^{2+} with dioctahedral smectite, are rare. Here we present a summary of the relevant experiments known to us. Most of the recent studies stem from the French radwaste program.

/Müller-Vonmoos et al. 1991/ (also reported in /Madsen 1998/) investigated the interaction of montmorillonite with magnetite and iron powders under H_2-saturated steam in autoclaves at 80°C for about half a year. The relative humidity was maintained at 75–99%. They found no evidence of Fe uptake by the clay or transformation of the expandable fraction. This result is probably explained by the absence of transformations under vapour conditions.

The effect of an Fe(II) silicate on bentonite properties under oxic and anoxic conditions was examined by /Oscarson and Heimann 1988/. They found a decrease in CEC and an increase in Fe^{2+}/Fe^{3+} for reacted samples under anoxic, but not under oxic conditions. The result was interpreted as precipitation of Fe-hydroxide at clay edges.

There is some early reported work on the formation of hydroxyl interlayers (chloritisation) in smectites at low temperatures /Rich 1968, Carstea 1968, Carstea et al. 1970/. Based on interaction experiments with smectitic materials and Al and iron salts as well as observations in soils (generally under oxic conditions), these studies suggest that Al-hydroxy interlayer complexes may be stable, whereas Fe-hydroxy layers are poorly developed and, furthermore, require particular conditions (e.g. low pH). At conditions more representative of the NF, the formation of separate Fe (hydr)oxide phases was also reported in the aforementioned studies.

/Lantenois 2003/ contacted smectites of variable Fe content with iron powders and degassed distilled water at low solid/liquid ratio (0.04) at 80°C for 45 days. The results indicated dissolution of smectite and formation of magnetite, an iron-rich clay phase (Fe^{2+}/Fe^{3+} ratio ≈ 1), and an iron silicate gel (Fe^{2+}/Fe^{3+} ≈ 0.25). The newly formed iron clay was identified to be a 1:1 clay with a composition close to cronstedtite. The conversion reaction was dependent on the initial Fe^{3+} content in the octahedral position, the expandability of the clay and the presence of a tetrahedral charge in the starting smectite. Thus, the reaction with Fe-rich nontronite (which contains a substantial tetrahedral charge deficit) was most extensive, followed by beidellite (with less Fe^{3+} than nontronite), and then montmorillonite. Iron-poor saponite did not react within the experimental time period. Smectite samples which had been exchanged with K^+ showed much less reactivity than the Na^+ and Ca^{2+} dominated ones. The observed Fe-clays were similar to the "berthierine" described by /Habert 2000/ who had contacted smectite/kaolinite mixed layers with Fe(0) at 80°C under aerated conditions. This suggests that the redox conditions were not entirely reducing in the experiments of /Lantenois 2003/. /Lantenois 2002/ invoked the same type of formation products for a FoCa clay exposed up to 170°C for four years at the Stripa site.

In the PhD study of /Guillaume 2002/, MX-80 bentonite was contacted with iron plates and magnetite and with magnetite and hematite at 80°C and 300°C under N_2-degassed conditions for periods up to nine months. The solid/liquid ratio was moderate (0.1). After the experiments, samples were prepared and stored under Argon. At 80°C, no mineralogical transformation was noted but a slight Fe^{3+} enrichment in the clay was observed. In the experiments with metallic iron and magnetite, a Fe^{3+}-enriched smectite of a nontronite-type formed. At 300°C and in the presence of magnetite and hematite, the starting montmorillonite got transformed to a high charge smectite enriched in Fe^{2+} and accompanied by the formation of quartz, feldspar and zeolites. At 300°C and in the presence of Fe(0) and magnetite, a high-charge smectite and an Fe^{2+}-rich chlorite formed. This transformation was shown to occur via smectite-chlorite irregular mixed layers. Concomitantly, rapid dissolution of trace minerals (e.g. carbonates) and the precipitation of quartz, feldspar and zeolites were observed. The pH after reaction was quite low (5–6). This work was published in /Guillaume et al. 2003, 2004/.

A preliminary study performed within the same group /Cathelineau et al. 2005/ involved further experimental study of MX-80 reactions with Fe and magnetite powder at variable solid/liquid ratios at 80°C under N_2-degassed conditions for about one year. It was shown that under conditions of higher reactivity (high surface areas, low S/L) bertherine-type phases with high Fe^{2+}/Fe^{3+} ratio were formed.

/Wilson et al. 2006a/ exposed purified Kunipia bentonite and iron compounds at low S/L ratio in NaCl solutions in an N_2 atmosphere for about 100 days. In the first series, Na-montmorillonite was contacted with Fe(0) and magnetite powders and calcite at 250°C. The resulting products were magnetite, hematite (in some runs), an altered Fe-rich smectite and zeolite (analcime). Based on solute concentrations and thermodynamic modelling, the altered smectite, that showed reduced expandability, was postulated to be an Fe-rich saponite. In the second series, Na-montmorillonite was contacted with Fe(0) powder and $FeCl_2$ at 80–250°C. In those tests, significant smectite alteration was only observed at 250°C. The reaction products were magnetite (and in some runs lepidocrocite) and a small proportion of a newly formed 1:1 Fe-clay.

The resulting pH values were low (4.2.–4.7). Based on solute concentrations and thermodynamic modelling, the newly formed Fe-clay was suggested to be berthierine.

/Carlson et al. 2006/ performed anaerobic corrosion experiments using cast iron and carbon steel coupons (9 cm^2 total surface area in each test cell) and carbon steel wires (0.1 m^2 total surface area in each test cell) in compacted Wyoming betonite (MX-80; 2 g/cm^3). The tests were run at 30° and 50°C in a background electrolyte of artificial ground water (0.54 mole NaCl + 0.01 mole Na_2CO_3/L, pH 10.4) and had a duration ranging from one to almost three years. After the tests the corrosion products on metal surfaces as well as the bentonite matrix were examined using a wide range of analytical techniques, such as scanning electron microscopy (SEM-EDX), XRD, Laser Raman spectroscopy, Fourier Transformed Infrared spectroscopy (FT-IR), transmission electron microscopy (TEM-EDS) and Mössbauer spectroscopy. In addition more conventional analyses including measurement of cation exchange capacity, total chemical composition by ICP-AES (after fusion and dissolution), swelling pressure and hydraulic conductivity were conducted. The results of the Carlson et al. study can be summarised as:

- The corrosion products on metal surfaces were found to consist of a mixture of magnetite, hematite and goethite. However, the layer of corrosion products was thin compared to what is normally observed on samples tested in aqueous conditions with no bentonite present, which suggested that a large part of iron released by corrosion entered into the bentonite rather than forming solid corrosion products.
- The analyses of the bentonite confirmed that iron had been incorporated in the bentonite matrix. The incorporated quantity was considerably higher in samples that represented conditions of higher reactivity, i.e. in the bentonite with wires. In these samples, a loss of cation exchange capacity and an increase in hydraulic conductivity were observed. In addition, the Fe^{2+}/Fe^{3+} ratio had increased by a factor of two or more compared with fresh bentonite, which, in part, was a result of the reduction of some octahedral iron in the montmorillonite. The green colour of bentonite in combination with the FTIR pattern suggested that some octahedral iron in the montmorillonite structure had been reduced during contact with metallic iron.
- Mössbauer analysis indicated the presence of adsorbed or absorbed Fe(II) and the fact that iron was very heterogeneously distributed within single montmorillonite aggregates was suggested to be due to some kind of surface coating. However, none of the techniques applied were able to detect any discrete neoformed iron-rich clay minerals or to identify any corrosion products within the bentonite matrix.

A summary of the recent studies is given in Table 2-1.

2.3.3 Information from natural analogues

Natural analogues that represent conditions of iron-bentonite interactions in an EBS are rare. Thus, useful natural analogue data is very limited /Marcos 2003/. Some insight can be gained from the occurrence of Fe-bearing mineral assemblages, as shortly described in Section 2.3.1. The most relevant information is summarized here:

Fe-rich smectite (e.g. nontronite, Fe-saponite) may occur in a variety of geological settings, but generally not in sediments rich in dioctahedral low-charge smectite. Nontronites form both in low temperature and hydrothermal systems of intermediate redox conditions. Fe-rich saponites are often formed at higher temperatures under hydrothermal conditions and are frequently associated with nontronite and celadonite.

The 1:1 Fe-phyllosilicates, such as berthierine and cronstedtite, are also found in a variety of environments and are often associated with ironstones. Berthierine forms mixed layers with chlorite and it has been reported by several authors /e.g. Mata et al. 2001, Aagard et al. 2000/ that berthierine acts as diagenetic precursor to chlorite. The transition from berthierine to chlorite in diagenetic sediments occurs at temperatures of 70–130°C /Aagard et al. 2000/.

Table 2-1. Experimental data on transformation of smectite in contact with reduced iron. S/L: solid/liquid ratio.

Reference	Experimental conditions	Neo-formed iron phases
/Madsen 1998/	MX-80 bentonite + Fe/Fe_3O_4 powder Clay/Fe^0 = 1, S/L = 0.1, t = 180 d, T = 80°, water vapour	none
/Lantenois 2003/	Various pure smectite minerals + Fe powder Clay/Fe^0 = 1, S/L = 0.04, t = 45 d, T = 80°	magnetite*, cronstedtite ("berthierine")
/Guillaume et al. 2003, 2004/	MX-80 bentonite + Fe/Fe_3O_4 powders Clay/Fe = 10, S/L = 0.1, t ≤ 9 months, T = 300°C	chlorite, saponite
	same, T = 80°C	nontronite
/Cathelineau et al. 2005/	MX-80 bentonite + Fe/Fe_3O_4 powders S/L varied, T = 80°C, t ~ 1 a	berthierine
/Carlson et al. 2006/	Compacted MX-80 bentonite + Fe coupons or wires Clay/Fe ~ 1, S/L = 3.6, t ≤ 900 d, T = 30 and 50°C	magnetite*, hematite*, goethite* no Fe silicate detected
/Wilson et al. 2006a/	Na-montmorillonite, Fe and Fe_3O_4 powders, calcite, S/L = 0.01, t ~ 100 d, T = 250°C	Fe-rich smectite (from solute conc. Fe-saponite proposed)
	Na-montmorillonite + Fe powder $FeCl_2$ solution, S/L = 0.01, t ~ 90 d, T = 80–250°C	magnetite*, hematite*, at 250°C: 1:1 clay (from solute conc. berthierine proposed)

* Corrosion products formed.

Chloritisation of smectites is a common phenomenon in sediments, but occurs at rather elevated temperatures of 150–200°C. It is important to note that this reaction involves high-charge smectites, such as saponite, which often forms irregular or regular (corrensite) mixed layer with chamosite. The formation of berthierine as intermediate phase may be involved in the transition of saponite to chlorite /Mata et al. 2001/.

Natural bentonites contain variable amounts of iron, which occurs predominantly in the Fe^{3+} state. As reported by /Marcos 2003/, there are some indications of bentonites rich in structural Fe^{2+}, (e.g. Greek bentonite from Kimolos and Milos, see /Christidis and Scott 1997/ but their formation mode is obscure, partly due to re-oxidation by surface alteration. The swelling capacity has been shown to be lower for the reduced relative to the oxidised bentonite fraction /Foster 1953, Stucki et al. 1984b/.

Interesting natural analogues may be altered meteorites rich in metallic iron (chondritic meteorites). A quick literature search, however, did not allow any conclusive statements on this topic. Nonetheless, some reported observations are of interest. The primary material consists of metallic iron containing variable amounts of Ni, which is embedded in a silicate spherulitic matrix. Main alteration products include various iron sulphides. Once sulphur is depleted, iron-rich silicates, such as cronstedtite, berthierine, chlorites and Fe-rich smectites have been reported to form /Zolensky and McSween 1988, Tomeoka et al. 1989/. A thorough literature review on the subject would be useful to obtain more comprehensive information on the interaction between iron and clays under reducing conditions.

2.3.4 Modelling studies on smectite-Fe interactions

To our knowledge, very few modelling studies exist in this area, which is not surprising given the limited experimental data. In a recent thermodynamic study by /Wilson et al. 2006b/, the stability fields of Fe-rich phyllosilicates were calculated in the system Al_2O_3-FeO-Fe_2O_3-MgO-Na_2O-SiO_2-H_2O (example given in Figure 2-3). The thermodynamic data were derived from the thermodynamic model for clays of /Viellard 2000/. According to the thermodynamic modelling presented by /Wilson 2006b/, Fe(II)-rich saponite and/or berthierine would be the stable Fe-clay

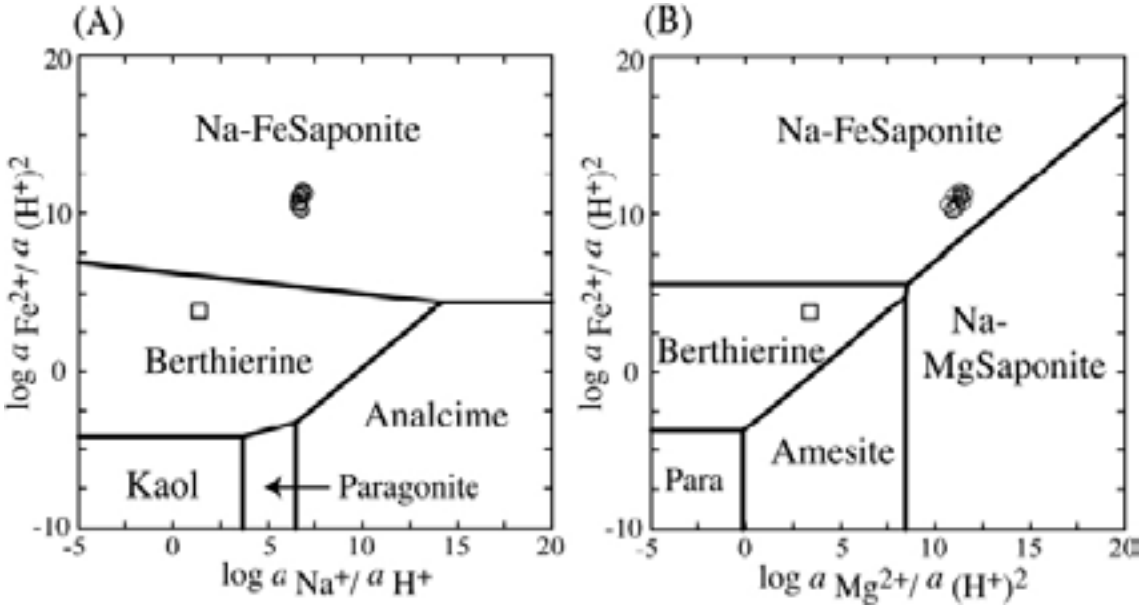

Figure 2-3. *Solute activity ratios on activity diagrams at (T = 250°C, $loga_{SiO2(aq)}$ = –3) for systems Al_2O_3-FeO-Na_2O-SiO_2-H_2O (A) and Al_2O_3-FeO-Na_2O-SiO_2-H_2O (B). Points denote experimental data. Taken from /Wilson et al. 2006a/.*

minerals under most repository situations. However, the authors concede that the underlying thermodynamic data that led to this conclusion are subject to considerable uncertainty.

The reaction between the steel canister and MX-80 bentonite in the French HLW concept was simulated /Andra 2005/ with the coupled diffusion-reaction model KIRMAT /Gérard et al. 1998/ that includes kinetics. An "in house" thermodynamic database that also includes clay phases (treated as solid solutions) was used. A constant temperature of 100°C and fully saturated conditions were assumed. The simulations that were run up to 3,300 years indicate very little transformation, the main one being the conversion of Na-smectite to Ca-smectite via ion exchange reactions. Minor neo-formation of illite and chlorite were predicted as well as re-precipitation of quartz and feldspar. The modelling exercise was recently extended to timescales of 50,000 years /Fritz et al. 2006/. The results indicate very limited transformation of montmorillonite to non-swelling Fe-rich silicates restricted to the first few cm of the contact area. The distribution of mineral phases at t = 0 and after t = 50,000 years is illustrated in Figure 2-4. The main clay transformation products resulting from the iron-bentonite interaction were found to be Fe saponite, Fe(II)-rich chlorite, the main corrosion product was magnetite.

A preliminary modelling study was performed at CEA Cadarache /Bildstein et al. 2006/ to describe the interaction of the canister with bentonite in the French EBS system. The model included 1D diffusion, chemical equilibria and dissolution/precipitation kinetics using the Crunch code and the Chess thermodynamic database. The results showed a clogging of the porosity due to mineral precipitation close to the canister-bentonite interface after a few thousand years, preventing further reactions. The main corrosion product to form was found to be magnetite, the main clay mineral transformation product was cronstedtite.

2.4 Effects on physical properties

The unaltered bentonite buffer provides several advantageous physical properties regarding repository performance:

- High swelling pressure and swelling capacity.
- Low hydraulic conductivity.
- Favorable rheology.

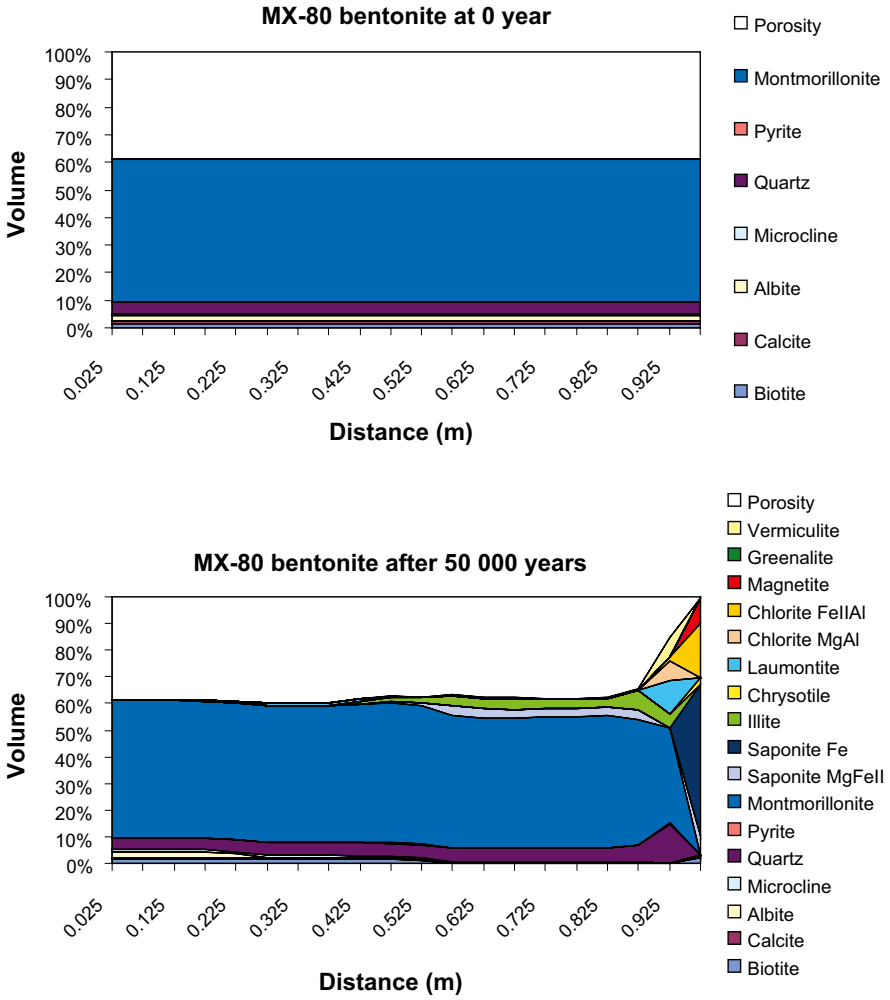

Figure 2-4. *Outcome of modelling study on bentonite-iron canister interaction of /Fritz et al. 2006/.*

An important question is how, and to what extent, the iron-bentonite interaction influences these properties. The nature of the impact on physical properties can be categorized into two broad groups:

- **Changes due to explicit transformation of montmorillonite**
  Basically all of the advantageous bentonite-specific physical properties stems from the ability of water molecules to enter interlayer spaces of the montmorillonite and hydrate the counter ions. In many of the transformed minerals resulting from Fe-montmorillonite interaction, water no longer has access to these spaces e.g. due to irreversible collapse of the original clay layers. Thus the swelling ability is lost, or strongly reduced, and a large increase in hydraulic conductivity is expected.
- **Cementation effects**
  The term "cementation" is usually defined in the context of formation of sedimenttary rocks, e.g. when grains of quartz are "glued" together by precipitating silica to form sandstones. However, in the case of highly compacted (saturated) bentonite, pore space is not distributed in such a way that precipitation is likely to occur without the clay itself playing a chemically active part. In the present context, we use the term "cementation" in a broad sense to describe effects of chemical and mineralogical processes which can lead to various changes in the rheological properties of the buffer material, for example increased mechanical strength, brittleness or reduced swelling capacity. A number of completely different processes could conceivably cause similar effects, and the underlying reactions can occur directly in the montmorillonite, in the interlayer space or in accessory minerals.

Clearly, an overlap exists between the two defined categories of impact on physical properties. It is also likely that the two mechanisms will occur in sequence, e.g. precipitation of silica released from the montmorillonite-to-berthierine transformation. Furthermore, iron compounds are well known to act as cement in ordinary soils under oxic conditions. In the case of anoxic conditions in bentonites, the effect of precipitating iron compounds is not clear and further investigation is needed.

2.4.1 Swelling pressure

Assuming no cementation effects, the magnitude of swelling pressure in saturated montmorillonite can be directly related to the (mean) interlayer distance of separate clay layers /Karnland and Birgersson 2006/. The impact of a mineral transformation on swelling pressure will therefore depend on the induced change of ratio between remaining montmorillonite and water. The effect is illustrated in Figure 2-5 in the case of chloritisation. Picture A shows an unaltered, water saturated Na-montmorillonite at a buffer density of 2,000 kg/m^3 (corresponding to a dry density of ~ 1,570 kg/m^3). The distance between the montmorillonite layers at this density is approximately 8 Å with a corresponding swelling pressure of ~ 7 MPa. The effect of chloritisation is exclusion of water from interlayer pores and reduction of interlayer thickness to approximately 4 Å, thus increasing the mean layer distance for the remaining unaltered montmorillonite (picture B) and lowering of the swelling pressure. The rightmost picture shows the result of a complete chloritisation; the swelling pressure is lost and the pore structure is completely changed with larger voids appearing.

Figure 2-6 shows calculated and measured swelling pressures as a function of density for MX-80 bentonite in contact with solutions of various salinities. The expected swelling pressure at buffer densities (~ 7 MPa at a dry density of ~ 1,570 kg/m^3) is indicated by the green arrow. The red arrow shows the impact of an effective density reduction due to 50% chloritisation (illustrated in Figure 2-4). For this unrealistically large montmorillonite conversion, the pressure reduction is seen to be substantial but the pressure will still above 1 MPa also for a 0.3 M NaCl-solution.

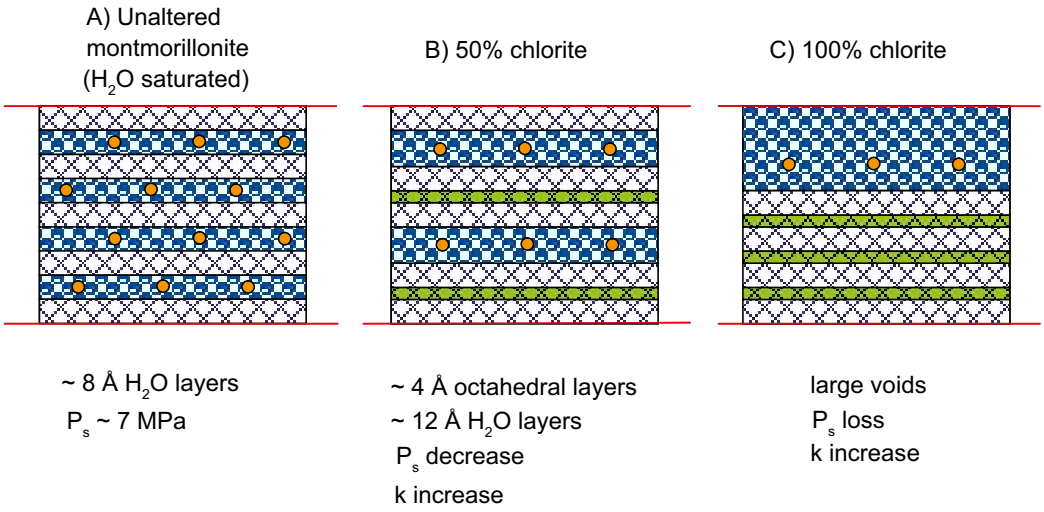

Figure 2-5. *Cartoon of water conditions in the montmorillonite interlayers. P_s indicates swelling pressure and k indicate hydraulic conductivity. Picture A shows the maximum cation hydration of unaltered montmorillonite in a limited space. The checkered, uncolored areas represent the tetrahedral-octahedral-tetrahedral layers, while water and cations are represented by balls. 50% chlorite (B) shows the collapsed interlayers and non-collapsed layers further hydrated. The additional octahedral hydroxide layers of chlorite, replacing water in the collapsed layers, are represented by green-checkered areas. 100% chlorite (C) shows the totally collapsed interlayers and large voids over which no force interaction with the surroundings particles exist /Karnland and Birgersson 2006/.*

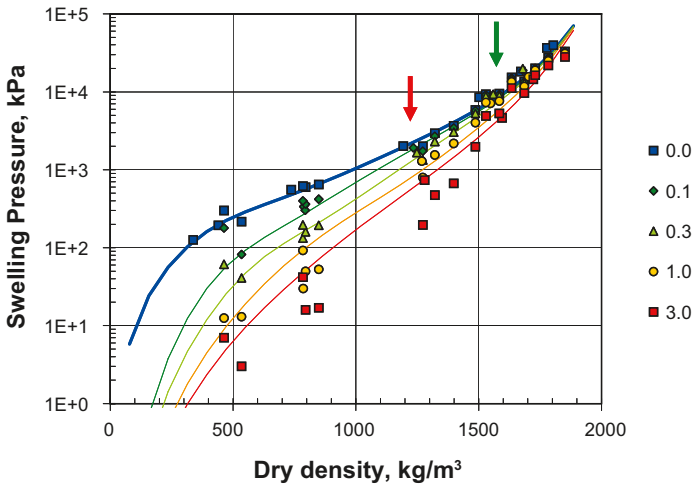

Figure 2-6. *Swelling pressure of MX-80 material in contact with pure water and NaCl solutions (0–3M NaCl). Dots show measured values. The green arrow (right) indicates the swelling pressure of unaltered buffer material at KBS-3 target dry density whereas the red arrow (left) illustrates the pressure at a 50% choritization (compare picture A and B in Figure 2-5).*

The impact on swelling pressure of iron-bentonite interactions has been investigated in only a few cases. By reducing the structural iron, /Stucki et al. 2000/ found a minor drop in the swelling pressure of two Na-smectites with very different amounts of structural iron. They explain the effect by layer collapse due to a layer charge increase induced by the reduction of structural Fe(III). This conclusion seems questionable however, as the total layer charge of the two smectites after reduction differs greatly. Such a large difference should result in completely different behavior regarding layer collapse and hence regarding swelling pressure reduction. /Carlson et al. 2006/ (the study is briefly described in Section 2.3.2) found moderate or no changes in swelling pressure in the test where iron coupons or wires were mixed with MX-80 and allowed to react at different temperatures and during different time spans. These results are presented in Figure 2-7.

Even if the swelling pressure can be sustained for significant buffer alterations it is important to differentiate between swelling pressure and swelling capacity. In the hypothetical case where the volume of the alteration products is large enough not to change the montmorillonite/water ratio, the swelling pressure will remain constant even though montmorillonite is consumed in the process. The swelling capacity, however, always lowers as montmorillonite is being consumed.

2.4.2 Hydraulic conductivity

The MX-80 reference results in Figure 2-7 show that the hydraulic conductivity of standard bentonite is directly related to the interlayer distance of clay layers, decreasing with increasing density. One contribution to this conductivity change comes from the pure volumetric effect of changing porosity. However, the major contribution is an effect of the strong density dependence of the surface/volume ratio of the interlayer pores at buffer densities, as can be seen in picture A and B of Figure 2-5. This ratio largely determines the size of interactions between water and clay surfaces and between water and counter ions, which in turn governs hydraulic conductivity. Thus, as a mineral transformation lowers the montmorillonite/water ratio, the hydraulic conductivity is expected to increase.

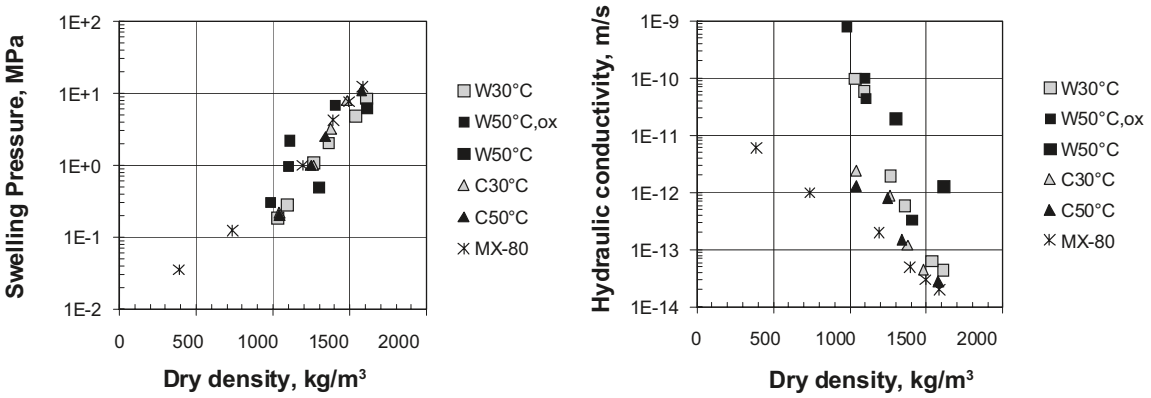

Figure 2-7. *Measured swelling pressure (left) and hydraulic conductivity (right) as a function of reduced clay dry density in the study of /Carlson et al. 2006/. C indicates coupon samples, W indicates wire samples, W50°C, ox indicates a slightly oxidized wire 50°C material. Figures in labeles denote temperatures. MX-80 shows reference values of typical untreated Wyoming bentonite.*

The character of the transformation products will also influence the resulting hydraulic conductivity. If these can be considered impenetrable isolated grains, they will contribute to a lowering of the hydraulic conductivity as an effect of the lowered porosity. If, on the other hand, grains of transformed minerals form porous subsystems in the bentonite, these tend to be more permeable than the remaining montmorillonite. Thus, preferential paths will be formed and hydraulic conductivity is expected to increase more than what is expected from just considering the montmorillonite/water ratio.

The above discussion points out the important fact that hydraulic conductivity in systems like these is not directly related to porosity. A complete chloritisation, for example, will result in a system with lower porosity than the original buffer (picture C in Figure 2-5). However, the hydraulic conductivity will be dramatically larger.

In the study by /Carlson et al. 2006/, a substantial increase in hydraulic conductivity was found in the samples treated with iron wires as shown in Figure 2-7. The increased conductivity indicates an inhomogeneous system with localized high-density volumes and low-density volumes since the swelling pressure was rather unaffected. All wires were removed from the samples before conductivity measurements were performed, but chemical analysis showed an increase of iron content from 2.4% (by mass) to 9.0% and 11.1% in the W30°C- and W50°C-samples respectively (see caption of Figure 2-7 for explanation of labels). The wire samples obviously contain iron corrosion products, but it is uncertain if this iron is located in transformed clay phases or in other iron precipitates.

Similar results showing unaffected swelling pressure but increased hydraulic conductivity were also found in bentonite material exposed to corroding iron in laboratory tests performed to simulate the conditions in a KBS-3H repository /Börgesson et al. 2005/. These experiments were, however, not performed under oxygen-free conditions.

/Shen et al. 1992/ showed changes in hydraulic conductivity as an effect of reduction of structural iron in two smectites with a large difference in iron content. The study was performed on soft gels (density ~ 0.2 g/cm^3) and the results might not be relevant at buffer densities for KBS-3 type repositories. They concluded that the effect of reduction depends on the history of sample preparation, but changes of sample densities were not considered in the evaluation, which makes the conclusion questionable. Similar to the study on swelling pressure by /Stucki et al. 2000/, we also question the interpretation that the conductivity changes are caused by iron reduction induced layer collapse as the effect is found to be rather insensitive to the huge difference in layer charge.

2.4.3 Rheology

Only the investigations mentioned in the previous sections of changes in physical properties as a result of Fe-interaction of bentonite have to our knowledge been reported, and the subject has to be considered as not comprehensively analyzed. Especially, quantification of the effects on buffer rheological performance due to cementation is completely missing. Carrying out such investigations would, however, demand rather extensive efforts considering experimental difficulties (working under oxygen-free conditions) and the variety of involved mechanisms.

2.5 Implications for the KBS-3H concept

As outlined in the above sections, there exist considerable uncertainties regarding the effects of iron-bentonite interactions on the integrity of the buffer. Nevertheless, the existing information enables constraining of the problem to some extent. In particular, the following implications hold for the KBS-3H repository concept.

2.5.1 Corrosion effects

The time of aerobic corrosion being short (maximum some decades), the degradation of the SC will be governed by slow anaerobic corrosion leading to hydrogen gas and magnetite. Of course, depending on the groundwater chemistry, iron sulphide and siderite could develop as well. Moreover, via the interaction with the clay, Fe(II)-silicate phases might form (see next section).

From the extensive corrosion data available, corrosion rates under anaerobic conditions are expected to be 1–2 μm a^{-1} in the compacted bentonite environment. The lifetime of the steel under these conditions will be rather short. For a rate of 1 μm a^{-1} (R), the time for complete corrosion (t_c) can be calculated:

$$t_c = \frac{d}{2R} = \frac{0.008\,m}{2 \cdot 10^{-6}\,m/a} = 4000\,a \qquad \text{(Equation 2-5)}$$

where d is the thickness of the supercontainer steel shell.

Due to the attack by sulphide, possibly enhanced by microbial activity, significant pitting cannot be ruled out. Localised corrosion is also favoured by the geometric configuration of the perforated SC (i.e. large number of machined holes). These effects, however, will not lead to a significant enhancement of the consumption rate of steel. Furthermore, the formation of a protective corrosion layer might also considerably slow down corrosion rates leading to an extended lifetime of uncorroded steel.

Because the area between the SC and the drift wall is small (≈ 4 cm thickness) at emplacement, a significant fraction may eventually be filled with iron corrosion products and Fe-altered clay (cf. next section). Due to volume expansion (if only magnetite formed, the volume would be approximately twice that of the original steel), the total porosity in this area is likely to be decreased relative to the unaffected buffer. On the other hand, the corrosion may adversely affect hydraulic properties in this interface area.

The effect of radiation on corrosion of the supercontainer steel shell will be negligible, since the canister will retain its integrity for a very long time. Even in case of an early canister failure, no significant effect of radiation on the SC is expected, due to the shielding provided by the bentonite buffer.

The corrosion products formed as a result of the SC corrosion will provide an additional sink for many radionuclides (e.g. ^{59}Ni, ^{79}Se, actinides) eventually released from the waste and diffusion through the bentonite buffer.

2.5.2 Fe-smectite interaction effects

Reduced iron is very reactive in contact with the smectitic clay and will interact via sorption and precipitation processes. The knowledge of these processes is still crude and large uncertainties exist on the effects on the bentonite material. However, some constraints can be defined:

- Fe(II) released by corrosion may end up in fairly insoluble corrosion products, such as magnetite and in the clay matrix. Thus, the amount of Fe reacting with the clay will be substantially constrained by the formation of magnetite, Fe(II) sulphide etc and by the slow mass transfer via diffusion into the bentonite.
- Sorption of Fe(II) released via the corrosion process to the smectite surfaces is fast and occurs both at the exchangeable interlayer sites and at the edge-type sites (SOH sites). Under repository conditions, Fe(II) will sorb predominantly to edge sites. It is presently unclear to what extent redox and co-precipitation (with Si and Al) processes are involved as a result of the Fe^{2+}-SOH interaction. Due to the strong sorption to the clay, competition of Fe(II) with other metallic radionuclides needs to be considered. Preliminary data suggest an enhancement rather than a weakening of sorption, but this point clearly needs to be further investigated.
- Due to thermodynamic and kinetic constraints, the transformation reaction of dioctahedral smectite to an Fe-rich clay phase is slow. During the initial thermal stage with temperatures above 60°C and time scales of less than 1,000 years, very limited transformation of the clay is expected. Hence, most of the potential transformation will occur over longer time scales at near to ambient temperature.
- The nature of the reaction products from the transformation of montmorillonite interacting with iron cannot be predicted accurately. Considering that conditions will be very reducing, available experimental data suggest, that the most likely phases to form are Fe-rich high smectite (e.g. Fe-saponite), berthierine and/or chlorite. In the first case, the effects on the bentonite properties are likely to be small. In the latter two cases, alteration of the expandable smectite may impair the physical properties of the affected region of the buffer.

2.5.3 Cementation effects

Laboratory tests have shown that iron-bentonite interactions may alter the buffer, e.g. by significantly increasing the hydraulic conductivity. If this is caused by explicit montmorillonite transformation or due to other precipitating iron phases remains unclear. No investigations directly aimed at elucidating the influence on mechanical properties of the buffer due to cementation from iron-bentonite interactions have been conducted.

3 Case study: The Olkiluoto site

The Olkiluoto site is used as a case study to estimate the effect of the supercontainer steel shell (SC) on the long-term performance of the bentonite buffer. Note that in addition to the SC, there are several other steel components foreseen in the design of KBS-3H: Compartment plugs, fixing rings and drip/spray shields. These additional steel components are not taken into account in the present study, because they will likely have a smaller impact on the buffer surrounding the canister than the supercontainer. Two approaches were adopted: (1) simple mass balance considerations and (2) geochemical modelling.

3.1 Mass balance calculations

The first straightforward approach to assess the effect of iron on the bentonite buffer is by using mass balance calculations and neglecting transport and geochemical constraints. The masses of bentonite and iron corresponding to one canister are listed in Table 3-1. The fractions of iron in the bentonite buffer, i.e. Fe mineral impurities and structural iron of the clay, are small compared to iron from the supercontainer steel shell.

Table 3-1. Iron fractions of different components in the NF.

	Mass [kg]	kmol keq	Comments
Buffer			
Total bentonite material [a]	16,129		Dry density = 1.56 Mg m^{-3} ε = 0.44, EBS dimensions given in Appendix A
Montmorillonite [b]	12,097	29.8	75wt%
Siderite, pyrite [b]	164	1.4	Assumption: 0.5% $FeCO_3$ and 0.5 FeS_2
Fe(III) oxide [c]	16.4	0.2	0.1% FeOOH
Structural Fe^{3+} [b]	338	6.0	
Structural Fe^{2+} [b]	16.9	0.3	
Cation exchange capacity [c]		3.4	75meq/100g bentonite
Edge sites [c]		0.5	15% of CEC
Steel supercontainer [a]	**869**	**15.6**	Length = 5,546 mm, thickness = 8 mm, perforation 60%, dimensions given in Appendix A

[a] Dimensions of EBS taken from /Johnson et al. 2005/. The present design includes non-perforated end-plates and a total mass of 1,071 kg /Autio et al. 2007/.

[b] /Müller-Vonmoos and Kahr 1983/ for Na-saturated form: $Na_{0.30}(Al_{1.55}Fe^{3+}_{0.20}Fe^{2+}_{0.01}Mg_{0.24})(Si_{3.96}Al_{0.04})O_{10}(OH)_2$.

[c] /Bradbury and Baeyens 1997/.

The impact of the iron structure on the swelling fraction of the buffer is assessed, assuming that all of the iron from the SC reacts with montmorillonite to form a non-swelling Fe-clay (see Section 2.3) by a simple mass balance calculation. In the first case it is assumed montmorillonite is transformed to berthierine via the simplified reaction:

$$Na_{0.25}(Al_{1.75}Mg_{0.25})(Si_4)O_{10}(OH)_2 + \mathit{1.75}Fe^0 + \mathit{2.125}H_2O + \mathit{0.75}H^+ \Rightarrow$$

$$\mathit{0.875}[(Fe_2Al)(SiAl)O_5(OH)_4] + \mathit{1.75}H_2 + \mathit{3.125}SiO_2 + \mathit{0.25}Mg^{2+} + \mathit{0.25}Na^+ \qquad \text{(Equation 3-1)}$$

Alternatively, if the reaction to chlorite (chamosite) is assumed:

$$Na_{0.25}(Al_{1.75}Mg_{0.25})(Si_4)O_{10}(OH)_2 + \mathit{4.375}Fe^0 + \mathit{6.5}H_2O + \mathit{0.75}H+ \Rightarrow$$

$$\mathit{0.875}[(Fe_5Al)(Si_3Al)O_{10}(OH)_8] + \mathit{4.375}H_2 + \mathit{1.375}SiO_2 + \mathit{0.25}Mg^{2+} + \mathit{0.25}Na^+ \qquad \text{(Equation 3-2)}$$

Thus, approximately 1.7 and 4.4 moles of Fe are required to convert one mole of montmorillonite into berthierine and chamosite, respectively. This reaction stoichiometry means that the SC, having 15.6 kmol of Fe, can convert at maximum 9.2 kmole or 3.5 kmol of montmorillonite depending on the assumed conversion reaction. In the case of the berthierine reaction, this amount is significant, corresponding to 30% of the total swelling fraction. In the chlorite reaction case, the loss of the swelling fraction would be 12%. The resulting reduction in swelling pressure can be estimated from the relationship between effective clay density and swelling pressure /e.g. Dixon 2000/. The effective clay density is defined as /e.g. JNC 2000/:

$$\rho_b = \rho_d\,(1–R_s)/(1–\rho_d R_s/\rho_s) \qquad \text{(Equation 3-3)}$$

where ρ_d is the bentonite dry density (Mg/m^3), R_s the fraction of the filling material and ρ_s is the grain density of the filling material. Upon 30% loss of swelling clay, the effective clay density would thus decrease from 1.56 to 1.32 Mg/m^3. Assuming 12% of loss, an effective clay density of 1.48 Mg/m^3 is derived. Taking the well-established relationship between density and swelling pressure /e.g. Dixon 2000/, the decrease in swelling pressure resulting from the complete iron conversion to Fe-clay can be estimated: At a density of 1.56 Mg/m^3, the swelling pressure is about 7 MPa which reduces to about 2 MPa at 1.32 Mg/m^3 and to 4 MPa at 1.48 Mg/m^3. Especially, for the berthierine case, such a change in swelling capacity is substantial.

It is important to note that above estimates overestimate the amount of swelling clay converted because:

- Corrosion reactions leading to the formation of magnetite or other insoluble Fe compounds will compete for Fe and significantly reduce the amount of Fe available for iron-bentonite interactions.
- Mass transfer is neglected in the mass balance calculations.

The outcome from the simple mass balance calculation highlights the need to apply a more sophisticated approach to bound the effects of iron on the buffer.

3.2 Geochemical processes in the KBS-3H environment

3.2.1 Geochemistry of the host rock

The geochemistry of the Olkiluoto site has been extensively investigated by geochemical and mineralogical analysis of a number of deep boreholes. /Posiva 2003, 2005, Andersson et al. 2007, Pitkänen et al. 2004/ give a comprehensive picture of the hydrogeochemical conditions at Olkiluoto.

The hydrochemical evolution is complex and strongly affected by the Quaternary history of the Baltic Sea. At least five different end-member water types (recent meteoric, recent Baltic, ancient Baltic = Litorina, glacial melt water and very old brine water) have influenced groundwater compositions by various degrees of mixing. While the upper part is characterised by a

dynamic hydraulic regime and a significant imprint of young meteoric waters, this is not the case for groundwaters below 300 m depth, which are characterised by glacial and older components. Fresh groundwater with low total dissolved solids (TDS ≤ 1g/L) is found at shallow depths, in the uppermost tens of metres. Brackish groundwater, with TDS up to 10 g/L dominates at depths varying from 30 to 400 m. The salinity gradually increases from 300 to 500 m depth and the water type gradually shifts from Na-Cl to Na-Ca-Cl, below 500 m, very old and highly saline waters (Ca-Na-Cl type) predominate.

The redox conditions are illustrated in Figure 3-1 (taken from /Pitkänen et al. 2004/). Microbially-driven sulphate reduction is the dominant redox reaction between 100 and 400 m depth, whereas methanogenesis, accompanied by high hydrogen levels predominates below 400 m. Isotope data suggest that at around 400 m concomitant sulphate reduction and methane oxidation occurs. In this zone sulphide is enriched (generally a few mg/L but up to 12 mg/L has been measured), whereas Fe concentrations are low. These species are controlled by metastable FeS and perhaps partly also by pyrite solubility. Pyrite coatings in fractures are frequent and constitute about 7% of the average coating area /Pitkänen et al. 2004/. Below 400 m, sulphide concentrations drop to insignificant levels, whereas Fe concentrations show an increase with depth, reaching several mg/L in the brine-rich waters. Iron in the fracture fillings occurs predominantly in the divalent state at greater depths and Fe(III) does not appear to play a significant role as electron acceptor.

The estimated Eh values in the sulphidic zone are in the range of –200 to –250 mV with respect to the SHE. In the methanogenic (carbonate reduction) zone, the Eh is estimated to be about –300 mV.

Microbial studies have been carried out on a few samples from deep boreholes /Haveman et al. 1998, 2000/ and recently from the shallow parts and overburden /Pedersen 2006, 2007/. Microbial activity was found to be low in the deep bedrock, which is typical for nutrient-poor deep crystalline environments. Sulphate-reducing bacteria were generally the most abundant species, but iron reducers were also detected. The presence of methanogens and acetogens was noted, but, because of the low amount of cultivatable cells, interpretation of these data is hampered. The presence of autotrophic methanogens (which use inorganic carbon together with hydrogen) in saline samples, together with high amounts of dissolved hydrogen and methane gases, indicate that carbonate reduction is an important process at great depths.

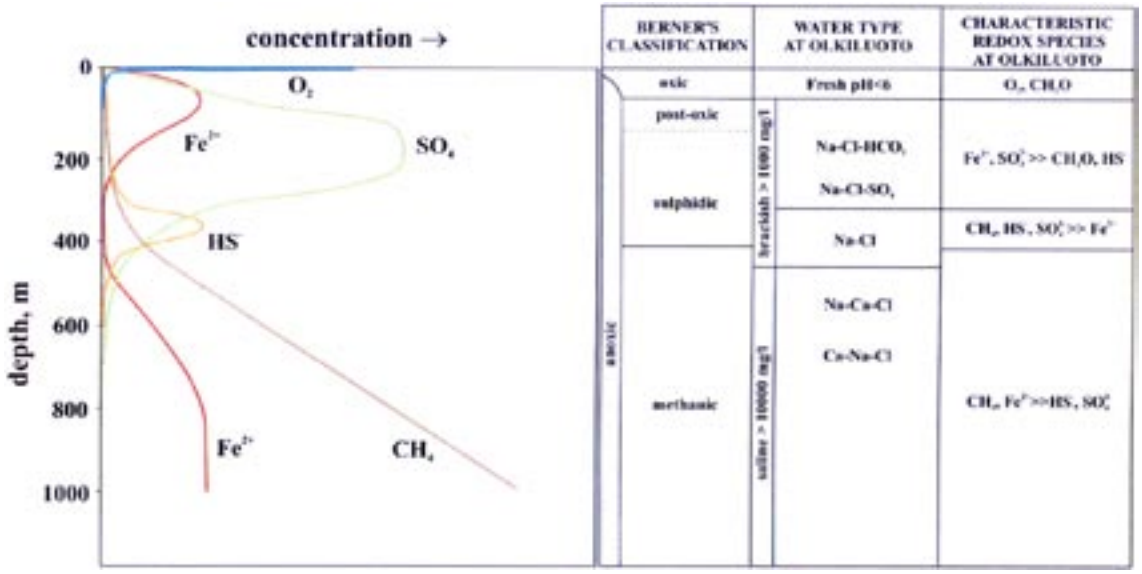

Figure 3-1. *Redox zones at Olkiluoto as function of depth /from Pitkänen et al. 2004/.*

Calcite is ubiquitous in fracture fillings and consequently groundwaters are close to saturation with respect to this mineral. The pH values are generally in the range of 7.5–8.5. Alkalinity and DIC show an increase with depth at shallower levels due to respiration processes. At levels below 200 m, a significant decrease of these parameters is noted which has been explained by mixing of different waters and calcite precipitation /Pitkänen et al. 2004/. Ca concentrations follow the reverse trend, thus obeying the calcite equilibrium condition.

Besides calcite, clay minerals (illite, smectite, kaolinite, vermiculite, chlorite) make up most of fracture filling. As mentioned above, pyrite is also abundant, mainly as coatings on calcite grains.

Due to continuing postglacial uplift, it is expected that fresher water will gradually displace saline water towards depth until the next glaciation.

In summary, the pH conditions in the deep aquifer system at Olkiluoto are well buffered by the presence of abundant carbonate and clay minerals. This is also true for redox conditions, which are buffered by the presence of iron sulphides and microbially-mediated redox processes.

Effect of repository on groundwater chemistry

The effect of the construction of the repository on the hydrologic and geochemical groundwater regime is subject to considerable uncertainty /Vieno et al. 2003/. Recent flow modelling /Löfman and Mészáros 2005, Ahokas et al. 2006/ indicates that construction will have a pronounced effect on the flow and salinity of the repository site ONKALO, situated at about 400 m in depth. Water inflow into the tunnel system is expected to lead to a drawdown of the water table and induce upconing of saline waters into the repository area, unless grouting measures are undertaken. Recent calculations (presented in /Pastina and Hellä 2006/) based on the assumption that tunnels are grouted to 1×10^{-7} m^2/s, suggest that salinity (Total Dissolved Solids, TDS) may rise up to 30–45 g/L at the lowest point of the tunnel system in ONKALO at depth of –550 m, whereas at the repository level (–420 m) the maximum salinity may rise from 4–12 g/L at emplacement to 10–25 g/L TDS during the operational phase /Pastina and Hellä 2006/.

By virtue of the large buffering capacity of the water-conducting fracture system, the disturbance induced by the operational phase should not lead to significant long term effects on Eh and pH conditions. The long-term evolution of the deep groundwaters may be influenced by glaciation effects, which may lead to upconing of saline water and/or dilution by inflow of fresher water /Vieno 2000, Vieno et al. 2003, Pastina and Hellä 2006/.

The inflow of massive amounts of oxic waters from the near-surface is unlikely, but has not been ruled at this point /Posiva 2003/. This scenario is not treated in this report.

Reference groundwaters

Based on the available data from deep boreholes /Pitkänen et al. 2004, 2007/ reference waters for repository conditions can be defined. All of the samples presented in Table 3-2 are classified as representative samples with no significant sampling or analysis uncertainties /Pitkänen et al. 2007/. The classification is based on integrated interpretation of hydrological background of sampling and chemical analyses of groundwaters. Samples from KR10, KR12 and KR6 are all classified as the most representative samples (B1) describing the baseline conditions at Olkiluoto in a reliable way, whereas the sample from KR20 is classified as B2, which means that it may contain water outside the test section, but is still representative for baseline conditions at Olkiluoto in the sampling depth of tens of meters. The sample has slightly elevated alkalinity/DIC and SO_4 and C-14 and H-3.

The two water samples KR20/465 and KR10/498 selected represent a more brackish and a more saline type, respectively. These selections are somewhat arbitrary, but are nonetheless deemed to reflect the expected range of compositions reasonably well once the site is constructed and natural conditions have been restored These two types and the water representing

Table 3-2. Compositions of groundwaters taken from selected measurements in /Pitkänen et al. 2007/. Calculated values obtained with Phreeqc assuming T = 15°C. Concentrations in mmole/L unless otherwise indicated. SI: saturation index.

	Reference waters		Limiting saline water	Limiting dilute water
Sample	**KR20/465/1**	**KR10/498/1**	**KR12/741/1**	**KR6/58/1**
Depth (m)	465	498	741	58
TDS (mg/L)	10,544	22,099	49,483	1,026
Ionic strength (meq/L)	218	478	1,180	20
pH	7.4	8.0	8.2	7.6
Alkalinity	0.66	0.11	0.12	2.79
DIC	0.55	0.11	0.04	2.72
SO_4	0.21	0.01	0.05	1.31
Cl	180.5	380.8	863.2	10.4
Na	114.8	210.0	360.9	9.8
K	0.28	0.36	0.49	0.20
Ca	32.4	89.1	254.5	2.1
Mg	2.6	1.6	1.5	1.1
Sr	0.16	0.37	1.14	0.01
SiO_2	0.36	0.28	0.21	0.41
Mn	5.8E–03	7.3E–03	9.3E–03	
Fe	2.5E–03	2.0E–03	3.8E–04	0.024
S^{2-}tot	5.61E–03	3.12E–04	1.25E–03	6.24E–04
Calculated data				
Eh (mV)	–217 S(6)/S(–2)	–258 S(6)/S(–2)	–299 C(4)/C(–4)	–35 $Fe(OH)_3$/Fe(2)
SI(calcite)	0.03	0.06	0.57	0.00
SI(FeS_{am})	–0.34	–1.06	–0.11	0.00
SI(pyrite)	8.80	6.05	6.40	16.2
SI(siderite)	–1.72	–2.16	–2.11	0.34

dilute/brackish water conditions (represented by a sample taken at 58 m depth from borehole KR6) should well cover the expected conditions at the site at emplacement and the evolution from post-emplacement until the far future /Pastina and Hellä 2006/.

Also considered here are “brine” type saline conditions (represented by a sample at 740 m depth from borehole KR12) as limiting composition of the expected possible variations (Table 3-2).

3.2.2 Geochemistry of near field

Porewater composition of bentonite buffer

The reference buffer material is highly compacted Na-rich MX-80 bentonite clay (dry density = 1.56 Mg m^{-3}). Under saturated conditions, the main fraction of the interstitial water is “bound” water occurring in the interlayers and at the outer surfaces of the smectite and only a small fraction is “free”, i.e. not affected by the clay surface charge. The thermodynamic properties of this porewater, being strongly affected by the electric double layer of the negatively charged clay particles, are not fully understood. Nevertheless, simple thermodynamic models (that largely ignore these effects) appear to adequately describe the porewater composition. This adequacy has been shown for example by modelling of bentonite – water interaction experiments performed at VTT /Muurinen and Lehikoinen 1999/, which covered a large range of solid/liquid ratios.

In fact, a modelling exercise performed by /Curti and Wersin 2002/ and /Wersin 2003/ revealed that experimental data could be simulated by conventional ion exchange and surface complexation models /Wanner et al. 1994, Bradbury and Baeyens 1997/. Further-more, as shown by geochemical modelling, a high acid – base buffering capacity of compacted bentonite results from the high cation exchange and proton exchange capacity and the presence of calcite.

As a consequence, the bentonite porewater chemistry is expected to remain fairly stable over long time periods. The main change will be induced by the exchange of Ca for Na at the clay exchanger /Wanner et al. 1992, Bruno et al. 1999/. Irreversible processes caused by temperature gradients, such as illite formation or cementation, which would reduce the swelling capacity, are expected to be insignificant below 100°C /e.g. Pusch and Karnland 1990, Wersin et al. 2007, Karnland and Birgersson 2006/.

Table 3-3 shows the porewater composition for bentonite equilibrated with the two reference groundwaters and the two alternative waters given in Table 3-2. The conventional model of /Bradbury and Baeyens 1997/, as applied by /Curti and Wersin 2002/, under the constraint of constant pCO_2 was used in this case. The assumption that pCO_2 is constrained by the rock is justified if long term conditions are considered, because diffusion of dissolved CO_2 in bentonite is fast relative to the timescales of interest (> 10,000 years).

Table 3-3. Calculated bentonite porewater composition for different groundwater compositions. Concentrations in mmole/L unless otherwise indicated.

	Reference waters		Limiting	Limiting
	brackish type	saline type	saline water	dilute water
Solution composition				
Ionic strength (meq/L)	315	507	1,169	220
pH	7.82	7.66	8.03	7.39
Alkalinity	0.52	0.40	0.072	2.50
SO_4	34.9	22.6	11.9	74.2
Cl	185	386	924	15.1
Na	271	384	645	167
K	0.85	1.24	2.3	0.53
Ca	20.8	42.9	167	10.4
Mg	6.32	10.9	24.9	1.1
Surface species				
NaX	1,990	1,980	1,890	1,990
CaX_2	249	247	324	248
MgX_2	69.3	63.8	49.8	70.3
KX	23.4	23.0	22.1	23.5
SOH	221	234	203	250
SO^-	68.2	54.4	86.1	35.4
SOH_2^+	2.14	3.12	1.3	5.68
Eh calculation				
Fe	2.3E–3	4.2E–3	4E–03	0.04
S^{2-}tot	5.3E–3	4.8E–3	1.3E–03	–
Eh (mV)	–171 Fe_3O_4/FeS	–160 Fe_3O_4/FeS	–280 Fe_3O_4/FeS	–202 Fe_3O_4/$FeCO_3$

The results indicate that, due to cation exchange and dissolution of calcite and gypsum, some changes in composition relative to the groundwater will occur. The changes are obviously greatest in the case of the bentonite contacting the "dilute" groundwater where the equilibrium with the ion exchanger will lead to increased cation concentrations. It is important to note, however, that because of strong buffering of the clay surface and the presence of calcite, the pH conditions will remain remarkably stable. The main change predicted for long timescales is enrichment of Ca relative to Na on the exchanger.

Wyoming bentonite generally contains Fe(II) mineral impurities, such as pyrite and siderite /e.g. Müller-Vonmoos and Kahr 1983/. In addition, traces of iron (hydr)oxides /Baeyens and Bradbury 1997, Bradbury and Baeyens 2002/ are present. Because of the variability in bentonite composition and possible oxidation of Fe^{2+} during processing of the raw material, the relative amounts of reactive iron phases may vary considerably. Moreover, the smectite fraction in MX-80 typically contains about 2 wt% of structural iron, most of which is Fe(III) /Vogt and Köster 1978/.

The redox conditions in the near field will pass from oxic to anoxic after repository closure. The time frame of this transition will be restricted from a few years to a few hundred years at the maximum, as pointed out in Section 2.1.1.

Also, compacted bentonite acts as an efficient filter towards microbes (see Section 2.1.1). Thus, it is not expected that microbially-mediated sulphate reduction will occur in compacted bentonite.

The Cu canister will experience oxidative corrosion during the short oxic stage. Afterwards corrosion will be very slow and canister lifetimes are expected to exceed 100,000 years /e.g. King et al. 2001/2002/.

Impact of the steel components on geochemical conditions

The corrosion aspects of the SC have been discussed in Chapter 2. With regard to the Olkiluoto site, it is important to note that the porewater chemistry in the SC environment will be "conditioned" by the geochemical conditions of the adjacent host rock and the bentonite buffer.

Because of the slightly alkaline conditions, an inner magnetite-type oxide layer will build up. The thickness of this layer, however, depends on the concentrations of other anions (sulphide, carbonate), the reactivity of the clay and the impact of microbial action. Under conditions of sulphate reduction in the adjacent host rock, as expected for the reference scenario, iron sulphide precipitation will be favoured (Equation 2-2). In the case of upconing of saline waters (saline scenario), less sulphide is available for competing for the corroded iron, thus less FeS will form relative to magnetite. In the dilute water scenario (zone of Fe^{3+} reduction) corroded Fe^{2+} may react to form siderite, although carbonate levels will probably not be very high. In all scenarios the clay may react with iron to form iron-rich clay. However, from a thermodynamic perspective, the extent will probably be less important when significant sulphide concentrations arising from sulphate reduction are available to bind Fe(II). The Fe concentration close the SC will be controlled by solubility of the corrosion products and thus similar to those of the groundwaters.

Due to the reducing capacity of the reduced iron in the buffer environment, it is reasonable to assume that the corrosion products largely control the redox conditions. For the reference and saline scenario, it is assumed that magnetite and FeS are the main corrosion products that impose Eh conditions. The resulting Eh values are listed in Table 3-3. In the case of the dilute scenario, it is assumed that the magnetite/siderite assemblage influences the redox conditions.

The thickness of the corroded layer, and thus the increase in SC volume, depends on the molar volume of the corrosion phases. In the case of magnetite, the increase of volume is about a factor of two. For FeS and $FeCO_3$ the increase is 2.5 and 4.7 respectively. A much higher volume increase for corroded Fe incorporated in a silicate phase is calculated. Thus, assuming the formation of berthierine, the volume increase is a factor of 8. This increase will however be largely compensated by the breakdown of the reacting clay. Under the assumption that all steel is converted to magnetite a decrease in porosity of about 2% would arise. This would lead to a slight increase in swelling pressure from 7 to about 8 MPa.

3.3 Geochemical modelling approach

3.3.1 Introductory remarks

The reaction of the corrosion-derived Fe with the swelling clay will be affected by slow mass transfer, which will occur predominantly by diffusion. The assessment of the extent of this reaction with time thus requires a coupled diffusion-reaction approach.

The Fe^{2+} concentration at the source will be constrained by the low solubility of corrosion products, which in the reference and saline water scenarios are expected to be magnetite and iron sulphide. This will limit Fe^{2+} concentration to a few μmoles per litre (cf. Tables 3-1 and 3-2). In the dilute scenario, there might not be enough sulphide to precipitate Fe^{2+}, in this case the maximum Fe^{2+} concentrations would be constrained by siderite solubility. The Fe^{2+} concentrations would then be in the range of 10–50 μmoles per litre (cf. Tables 3-1 and 3-2).

The Fe(II) concentration in the buffer porewater not affected by the corroding SC, depends on the presence of Fe(II) impurities. If, for example, there are sufficient FeS impurities, the Fe(II) concentrations will be in the same range as released from the source containing iron sulphides. Thus, there will be barely any concentration gradient and diffusion of SC-derived Fe(II) will be exceedingly slow. If there are sufficient siderite impurities, then the Fe(II) concentrations in the buffer porewater will exceed those at the source and there will be a transport of Fe(II) towards the SC until all $FeCO_3$ is consumed. The only significantly unfavourable situation arises in the case where there is only a very insoluble Fe(II) phase or no Fe(II) impurities at all to dissolve in the buffer. In the latter case, some Fe(II) from the clay fraction would dissolve. The solubility of Fe(II) under such conditions is not known, because the controlling phase is not known and, moreover, the thermodynamic database for Fe(II)-containing phyllosilicates is rather crude.

Under conditions of a concentration gradient between the SC and the buffer, the diffusion of Fe(II) will be retarded by sorption and precipitation reactions. From the above sections it is obvious that knowledge of the iron-bentonite interaction processes is still limited, in particular with regard to clay transformation processes. Therefore, the following diffusion-reaction calculations serve as a bounding analysis rather than an accurate prediction of the geochemical evolution of the near field. Two types of modelling approaches have been performed. In the first, the iron front into the buffer has been assessed under the consideration of Fe(II) sorption with no clay transformation reactions (e.g. no Fe(II) clay precipitation). In the second, a more extensive reactive transport model including clay transformation reactions has been applied.

3.3.2 Modelling of Fe sorption front with Phreeqc

Model description

As presented in Section 2.2, there are some useful sorption data which can be applied to a sorption model for Fe(II) /Tournassat 2003, Charlet and Tournassat 2005/.

Diffusion-reaction calculations were performed under the assumption of unfavourable Fe^{2+} concentration gradients outlined above. Two test cases were considered (Table 3-4). In test case A, the iron source at the SC was assumed to be controlled by amorphous FeS solubility (with Fe_{tot} = 4 μmole/L) and a porewater composition corresponding to the more saline composition within the reference scenario. In case B, the siderite solubility constraint (Fe_{tot} = 40 μmole/L) and porewater composition corresponding to the dilute scenario was applied. Note that in this scenario the pH is lower than in the reference case and, as a consequence, Fe(II) sorption is less pronounced.

For both cases, sorption of Fe^{2+} was considered, taking the initial Fe^{2+} concentration in the bentonite porewater equal to zero. The basis for the geochemical modelling was the thermodynamic bentonite model described in /Curti and Wersin 2002/, which was briefly presented in Section 3.1.2. The considered sorption and mineral equilibrium reactions and the corresponding logK values are given in Table 3-5. The sorption reactions of Fe^{2+} to the clay were included by applying the data of /Tournassat 2003/.

Table 3-4. Input data used for modelling of Fe(II) sorption front.

	Test Case A	Test Case B
Diffusion coefficient D_e	2e–11 m^2/s	2e–11 m^2/s
Porosity	0.44	0.44
Dry density	1.56 Mg/m^3	1.56 Mg/m^3
Initial porewater chemistry	"Reference" water, brackish type (Table 3-3)	"Dilute" water (Table 3-3)
Fe(II) source concentration	4e–6 mole/L	4e–5 mole/L
Cation exchange capacity	75 meq/100g	75 meq/100g
Edge site concentrations	According to /Bradbury and Baeyens 1997/	According to /Bradbury and Baeyens 1997/

Table 3-5. Sorption and solid phase equilibrium reactions used in transport modelling.

Reaction		logK⁰	Reference/Comments
Cation exchange			CEC = 2.66 eq/L
$NaX + Ca^{2+}$	$\Leftrightarrow CaX_2 + 2Na^+$	0.415	/Bradbury and Baeyens 1997/
$NaX + K^+$	$\Leftrightarrow KX + Na^+$	0.60	"
$2NaX + Mg^{2+}$	$\Leftrightarrow MgX_2 + 2Na^+$	0.342	"
$NaX + Fe^{2+}$	$\Leftrightarrow FeX_2 + 2Na^+$	0.415	Tournassat (2003)
Surface complexation			SOH_{tot} = 0.399 eq/L
$S_sOH + H^+$	$\Leftrightarrow S_sOH_2^+$	4.5	/Bradbury and Baeyens 1997/
S_sOH	$\Leftrightarrow S_sO^- + H^+$	–7.9	"
$S_{w1}OH + H^+$	$\Leftrightarrow S_sOH_2^+$	4.5	"
$S_{w1}OH$	$\Leftrightarrow S_sO^- + H^+$	–7.9	"
$S_{w2}OH + H^+$	$\Leftrightarrow S_sOH_2^+$	6.0	"
$S_{w2}OH$	$\Leftrightarrow S_sO^- + H^+$	–10.5	"
$S_sOH + Fe^{2+}$	$\Leftrightarrow S_sOFe^+ + H^+$	5.0	/Tournassat 2003/
$S_{w1}OH + Fe^{2+}$	$\Leftrightarrow S_{w1}OFe^+ + H^+$	0.5	"
Solids			
$CaCO_3$	$\Leftrightarrow Ca^{2+} + CO_3^{2-}$	–8.48	Phreeqc Database
$CaSO_4\,2H_2O$	$\Leftrightarrow 2H_2O + Ca^{2+} + SO_4^{2-}$	–4.58	"
$SiO_2 + 2H_2O$	$\Leftrightarrow H_4SiO_4$	–3.98	"
FeS(ppt)	$\Leftrightarrow Fe^{2+} + S^{2-}$	–3.915	", used as input Fe for case A
$FeCO_3$	$\Leftrightarrow Fe^{2+} + CO_3^{2-}$	–10.89	", used as input Fe for case B

Diffusive transport was simulated with aid of a one-dimensional diffusion-reaction model:

$$\varepsilon \frac{\partial C}{\partial t} = D_e \frac{\partial^2 C}{\partial x^2} - \varepsilon \frac{\partial q}{\partial t} \qquad \text{(Equation 3-4)}$$

where C (mol kg^{-1} porewater) is the species concentration, t is the time (s), x is the distance (m), D_e is the effective diffusion coefficient (m^2 s^{-1}), ε is the porosity, and q is concentration in solid phase (mol kg^{-1} porewater). The modelling was performed with the Phreeqc Version 2 code /Parkhurst and Appelo 1999/, which solves transport by an explicit finite difference scheme. The chemical interaction term $\partial q/\partial t$ is computed separately for each time step and corresponds to the change in concentration in the solid phase.

The buffer is represented by a 40 cm wide column[1], divided into 20 cells of equal thickness (Figure 3-2). At the front end, a constant concentration boundary condition $C(0,t) = C_0$ (corresponding to the porewater in equilibrium with the corroded steel supercontainer) is imposed.

At the back end, closed boundary conditions ($\partial C(40cm,t)/\partial x = 0$) are assumed. A uniform effective diffusion coefficient of $2 \cdot 10^{-11}$ m^2 s^{-1} is assumed for all species /Yu and Neretnieks 1997, Gaucher et al. 2004/ reacting with the clay surface sites (which were pre-equilibrated with groundwater in a previous step) and the accessory minerals.

Results from diffusion-reaction calculations: major ions

Calculations were first performed without including the iron component. The results indicate relatively minor changes of the main composition with time for both test cases A and B (data not shown). There is some exchange of Ca for Na during the first few thousand years, which is mainly due to dissolution of gypsum. Once this phase is depleted insignificant changes occur. The pH conditions remained constant within 0.1 units for both test cases.

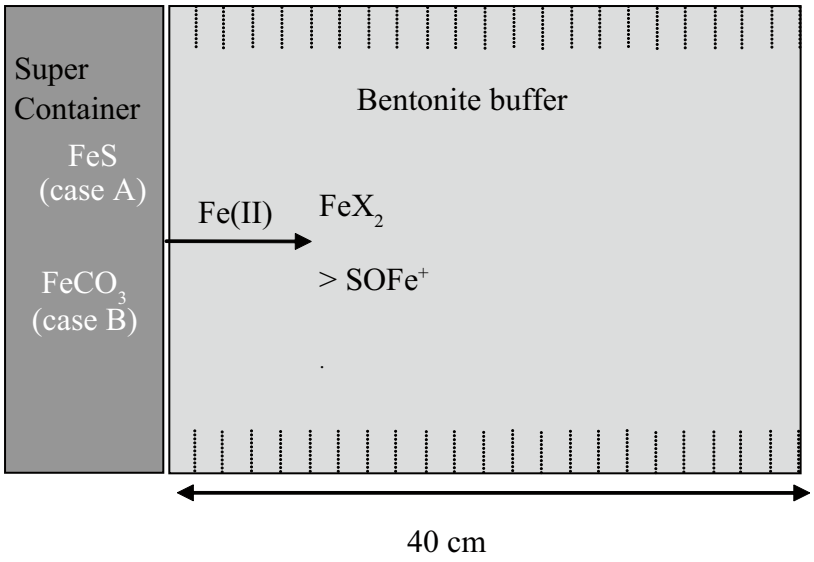

Figure 3-2. *Representation of steel supercontainer-buffer system in diffusion-reaction model.*

[1] In fact the buffer width inside the SC is 35 cm, and at emplacemnt there is a gap of about 4 cm between the SC and the rock, which will be filled with bentonite and corrosion prdoucts due to swelling of bufffer and corrosion of SC. Due to simpler representation, a 40 cm buffer width was used. The effect on the results is marginal.

Results from diffusion-reaction calculations: including Fe sorption

The calculated Fe migration behaviour for test cases A and B is illustrated in Figures 3-3 and 3-4. For test case A (control of Fe(II) source by FeS equation) the diffusion proceeds at a very slow rate. Thus, the breakthrough of the Fe sorption front at a penetration depth of 15 cm occurs after about 300,000 years. The breakthrough at the centre of the buffer (i.e. at the buffer/ Cu canister interface) occurs about 300,000 years later. Note that there is a considerable time lag between the sorption and dissolved Fe front because of the very high affinity for the clay surface.

For test case B, the diffusive flux is higher because of the steeper concentration gradient. Moreover, pH conditions are less alkaline, thus leading to less strong sorption. Therefore, breakthrough of the sorption front is predicted to occur after about 30,000 and 150,000 years for 15 and 30 cm depth respectively. Nevertheless, the results indicate effective retardation of iron even for this unfavourable case.

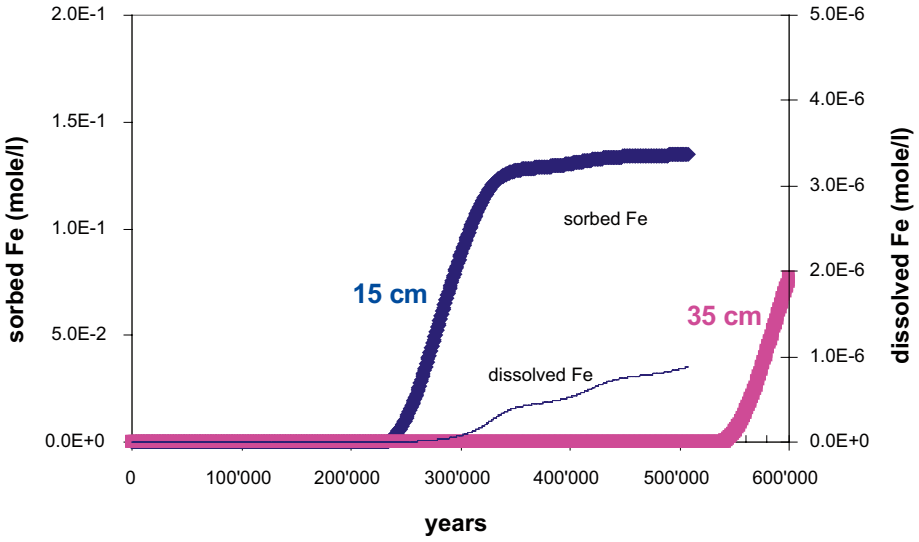

Figure 3-3. *Breakthrough curves of Fe(II) for test case A at 15 cm and 35 cm distance from the supercontainer steel shell; only sorption considered.*

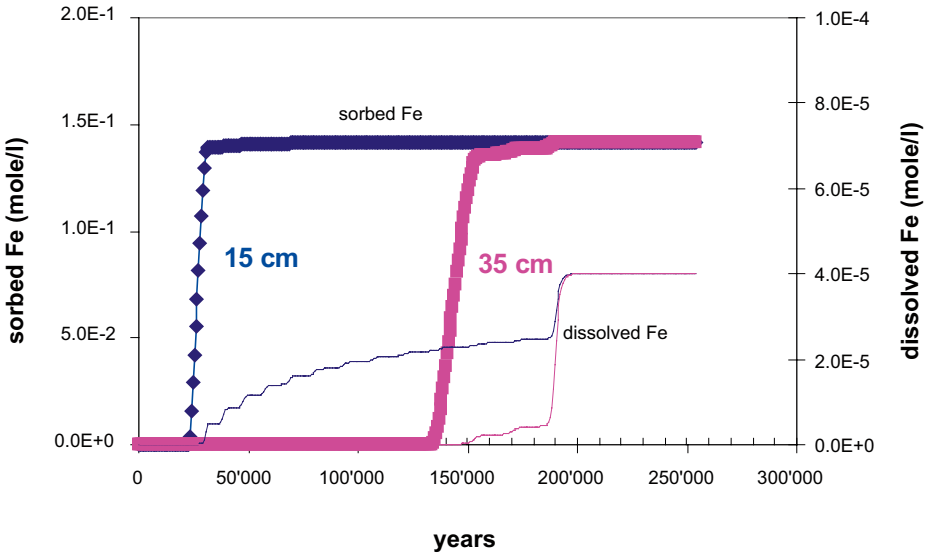

Figure 3-4. *Breakthrough curves of Fe(II) for test case B at 15 cm and 35 cm distance from the supercontainer steel shell; only sorption considered.*

The model predicts for both cases that most of the Fe is sorbed to the edge sites and only a small fraction is bound to the ion exchanger. We recall that the Fe sorption input parameters are taken from the experimental and modelling study of /Tournassat 2003/.

In summary, the diffusion-reaction calculations indicate very slow migration of Fe^{2+} derived from the supercontainer steel shell. In spite of the large uncertainties related to the interaction process between Fe and the clay, the results of these limiting cases illustrate the effective constraint imposed by diffusion and the low concentration gradient. The latter arises from (i) the low solubility of Fe(II) and (ii) the strong affinity of Fe for the clay.

3.3.3 Reactive transport modelling with CrunchFlow

Model description

A second geochemical modelling approach was carried out in which equilibrium and kinetic reactions for clay minerals were specifically included. In addition, the effect of the supercontainer steel shell corrosion reaction on the reaction pathway was analysed. The aims for this modelling exercise were:

- to obtain rough estimates of the spatial extent of the montmorillonite transformed by Fe-bentonite interaction as function of time,
- to estimate Fe fluxes and relative distribution of Fe species as a function of time,
- to explore the sensitivity of the results with regard to changing geochemical boundary conditions and parameter uncertainties.

All calculations were performed with the dilute water composition defined in Table 3-3, which constitutes the most unfavourable water chemistry in terms of Fe(II) transport and was used for test case B in the first modelling series.

Treatment of clay reactions

The thermodynamic data for clay phases is rather poor given the chemical complexity and small-scale variability of these phases and the slowness of dissolution/precipitation reactions, which makes reliable solubility measurements very difficult /e.g. May et al. 1986/. Because of this drawback, thermodynamic data used for geochemical applications are usually based on ΔG_f estimations from thermodynamic models. Various models exist in the literature, such as solid solution models /e.g. Aagard and Helgeson 1983, Tardy and Duplay 1992/ or ΔG models for discrete mineral phases /e.g. Mattigod and Sposito 1978, Chermak and Rimstidt 1989, Viellard 2000/. Here the selected thermodynamic data for smectites was based on the recent model of /Viellard 2000/, which is well accepted because of its rigorous treatment of thermodynamically consistent constituent oxide data /Meunier 2005, Andra 2005/. In this model, ΔG_f^0 of a smectite is based on the following expression:

$$\Delta G_f{}^0 = \sum n_i \Delta G_f{}^0 (M_i O_{x,i}) + \Delta G_{ox}{}^0 \qquad \text{(Equation 3-5)}$$

where the first term is the sum of Gibbs free energies of formation of the different constituent oxides. The second "interaction term" ΔG_{ox}^0 is the Gibbs free energy of formation from the constituent oxides of the smectite composition of interest and is based on the electronegativity of cations in the tetrahedral, octahedral or interlayer site.

For 1:1 clays, such as for the Fe-serpentines berthierine and cronstedtite, /Wilson et al. 2006b/ derived logK values from the model of /Chermak and Rimstidt 1989/. However, applying the logK value for berthierine in scoping calculations resulted in unrealistically low Fe(II) concentrations ($\approx 10^{-15}$ mol/L). In fact, taking different Fe phyllosilicate phases reported in the Lawrence Livermore National Lab (LLNL) database yielded equilibrium Fe(II) in the bentonite porewater in the range of 10^{-6} to 10^{-5} mol/L. In view of this, the logK was arbitrarily adjusted to a value that resulted in Fe(II) concentration of 10^{-6} mol/L.

The clay phases together with their stoichiometries and logK values used in the reactive transport calculations are presented in Table 3-6.

Table 3-6. Solid phase equilibrium reactions used in transport modelling.

Reaction	logK⁰	Reference/comments
Montmorillonite		
$Na_{0.2}Ca_{0.06}(Mg_{0.32}Al_{1.68})(Si_4)(O_{10})(OH)_2 + 6H^+ + 4H_2O \Leftrightarrow 0.2Na^+ + 0.06Ca^{2+} + 1.68Al^{3+} + 4H_4SiO_4$	5.096	calc. from /Viellard 2000/
Berthierine		"
$Fe_2Al_2SiO_5(OH)_4 + 10H^+ \Leftrightarrow 2Fe^{2+} + 2Al^{3+} + H_4SiO_4 + 5H_2O$	17.00	adjusted to Fe(II) = 10^{-6} M (see text)
Cronstedtite7A		
$Fe_2Fe_2SiO_5(OH)_4 + 10H^+ \Leftrightarrow 2Fe^{2+} + 2Fe^{3+} + H_4SiO_4 + 4H_2O$	16.26	LLNL database
Kaolinite		
$Al_2Si_2O_5(OH)_4 + 6H^+ \Leftrightarrow 2Al^{3+} + 2H_4SiO_4 + 1H_2O$	6.81	LLNL database
SiO_2(am)		
$SiO_2 + 2H_2O \Leftrightarrow H_4SiO_4$	2.71	LLNL database
Magnetite		
$Fe_3O_4 + 8H^+ \Leftrightarrow 1\ Fe^{2+} + 2Fe^{3+} + 4H_2O$	10.47	LLNL database
Quartz, Calcite, Gypsum, FeS, Siderite		see Table 3-5

The kinetic rate data for clay phases and other minerals such as quartz, SiO_2(am) and kaolinite was taken from a recent compilation of /Palandri and Kharaka 2004/. The work is based on the transition state theory for mineral kinetics /Lasaga 1998/, but applies a semi-empirical method to derive kinetic rate constants for common rock-forming minerals. It uses a variety of experimental data and proposes rather simple rate expressions that can be used both for dissolution and precipitation rates. For example, under near neutral conditions, the rate constant is expressed as:

$$\log k_{n,T} = \log A_n - \frac{E_n}{2.3RT} \qquad \text{(Equation 3-6)}$$

where A_n and E_n are the pre-exponential factor and the activation energy, respectively, valid for neutral conditions and $k_{n,T}$ is the zero-order rate constant for neutral conditions at temperature T. In order to account for the slowing down of the rate close to equilibrium, the authors propose to use the term $(1 - (Q/K)^p)^q$ where Q is the activity product, K is the equilibrium constant, and p and q are empirical parameters which are known for only a few minerals. /Palandri and Kharaka 2004/ suggest using 1 as first approximation for both exponents. Thus, for the complete reaction rate for neutral conditions:

$$Rate = \frac{dm}{dt} = S \cdot k_n^{T_0} \cdot \exp\left(\frac{-E_n}{R}\left(\frac{1}{T} - \frac{1}{T_0}\right)\right) \cdot \left(1 - \frac{Q}{K}\right) \qquad \text{(Equation 3-7)}$$

where dm/dt is the rate in mol/s, S is the surface area in m^2, and T_0 is the temperature at 298.15 K. Similar rate expressions are given for acidic and alkaline conditions.

In the present calculations, no use is made of the activation energy since $T = T_0$ in all considered cases, which is close to the expected temperature at the SC-rock interface in the time span after 1,000's of years, although elevated temperatures up to about 50°C are expected during the first 100's of years /Ikonen 2003/. The rate data used in our reactive transport calculations are given in Table 3-7. For the 1:1 Fe clay phases, the rate parameters for kaolinite were substituted, as these data are unavailable for berthierine and cronstedtite.

Table 3-7. Kinetic rate parameter used in transport modelling /from Palandri and Kharaka 2004/.

Mineral phase	$\log k_n^{T0}$ mol m^{-2} s^{-1}	E_n kJ mol^{-1}
Montmorillonite	–14.41	48.0
Kaolinite	–13.18	22.2
Berthierine	same as kaolinite	same as kaolinite
Cronstedtite	same as kaolinite	same as kaolinite
Quartz	–13.40	90.9
SiO_2(am)	–12.23	74.5
Magnetite	–10.78	18.6

Implementation in the CrunchFlow code

After performing several preliminary runs with Phreeqc, it became clear that this code had limitations for these types of reactive transport calculations (RTC). In particular, convergence problems resulted when slow kinetic reactions were included. Also, run times were long, taking several days for typical test calculations. Therefore the CrunchFlow /Steefel 2006/ reactive transport code was used instead. In contrast to Phreeqc, this code has the option of solving the transport and reactive part of mass balance simultaneously (global implicit method). Using CrunchFlow for these systems, calculation times were typically lowered by one order of magnitude or more and convergence problems were rare. As CrunchFlow is specifically aimed at RTC in porous media, it includes several advantageous features such as a porosity update when minerals precipitate or dissolve. The porosity, ε, in turn can be coupled to the diffusivity as

$$D_e = D_0 \varepsilon^m \qquad \text{(Equation 3-8)}$$

where D_0 represents the diffusivity for the initial porosity and m, the so-called cementation factor, is an empirical parameter. Furthermore, the form of the mineral dissolution/precipitation rate expression, given in equation 3-7 is implemented in the code.

Defining different test cases

Various test cases were defined in order to explore the sensitivity of different assumptions, boundary conditions and parameters in the reactive transport model. It should be kept in mind that the underlying data, mainly with regard to the clay reactions, is of rather large uncertainty. Moreover, as mentioned above, an adequate description of the corrosion process of the SC situated at the buffer/hostrock boundary and its coupling to iron-bentonite interaction processes proved to be difficult. Therefore, a limiting test case was defined for the corrosion process.

A summary of the test cases that were modelled is given in Table 3-8. Test case B represents the same situation as test case B as presented in the previous section for the Phreeqc calculations. This repeat modelling was performed in order to compare both codes. The initial porosity in the two cases differs slightly since CrunchFlow explicitly calculates this quantity from the specified list of initial minerals. In the following calculations, the diffusivity (D_0) has been changed accordingly, in order to obtain an initial effective diffusivity identical with the Phreeqc case. In the test case series C, a constant Fe(II) input flux was assumed, but clay reactions were taken into account. In the test series D, corrosion was explicitly included and clay reactions where switched on or off depending on the case. The input data for the various cases are depicted in Table 3-9. Because CrunchFlow explicitly calculates the number of exchange sites from the amount of montmorillonite and the specific surface area, the value of the cation exchange capacity differs from the value specified in Table 3-1.

Table 3-8. Compilation of test cases used in the CrunchFlow calculations.

Test case	Fe source	Clay reactions	Porosity update	Fe(II) sorption	Comments
B	Const. Fe(II)	No	No	Yes	To verify Phreeqc calc.
C0	Const. Fe(II)	Yes	Yes	Yes	
C1	Const. Fe(II)	Yes	Yes	Yes	No magnetite precip.
C2	Const. Fe(II)	Yes	No	Yes	No magnetite precip.
C3	Const. Fe(II)	Yes	Yes	Yes	Higher diffusion coefficient
C4	Const. Fe(II)	Yes	Yes	Yes	Higher montmorillonite solubility
D0	Corrosion	Yes	Yes	No	

Table 3-9. Input data used in the CrunchFlow calculations.

Parameter/feature	Value	Test cases
Diffusion coefficient D_0	4.5e–11 m^2/s	All, except C3
Initial Porosity	0.47	All
Exponent in $D_e = D_0\varepsilon^m$	m = 1	All
Dry density	1.56 Mg/m^3	All
Initial porewater chemistry	“dilute” water (Table 3-3)	All
Fe(II) source concentration	4e–5 mole/L	All, except D0
Cation exchange capacity	87 meq/100g montmorillonite	All (Table 3-1: 75 meq/100g)
Edge site concentrations	Bradbury and Baeyens model	All
Initial montmorillonite conc.	80.4 wt %	All
Initial quartz conc.	18.1 wt %	All
Initial calcite conc.	1.1 wt %	All
Initial gypsum conc.	0.4 wt %	All

Model descriptions and Results

Test Case B

This case was set up in order to verify that CrunchFlow reproduces the results from the previous Phreeqc modelling described in Section 3.3.2. A system identical to case B was set up and the geometry of Figure 3-2 was adopted. Figure 3-5 compares the iron concentration as a function of time at two different positions in the buffer from the Crunch Flow and Phreeqc calculations, respectively. Indeed it is verified that the Phreeqc results are reproduced. The slightly different slope of the curves as the iron front reaches the inner boundary (around 160,000 years) of the model is related to differences in the numerical schemes used by the two codes.

Test Cases C

The geometry depicted in Figure 3-2 was also used for these test cases where all precipitation/dissolution reactions were treated kinetically. Apart from the minerals already present in the buffer (see Table 3-9), magnetite, berthierine, siderite, anhydrite, cronstedtite, FeS(am) and amorphous silica were allowed to precipitate as well. A specific surface area of 37.5 m^2/g was used for montmorillonite (BET-value measured by gas adsorption) and a default porous media value of 100 m^2/m^3 was used.

In the following we examine the mineral distribution of the buffer after 100,000 and 500,000 years. In all cases, the calcite and gypsum, initially present in the buffer, were completely dissolved.

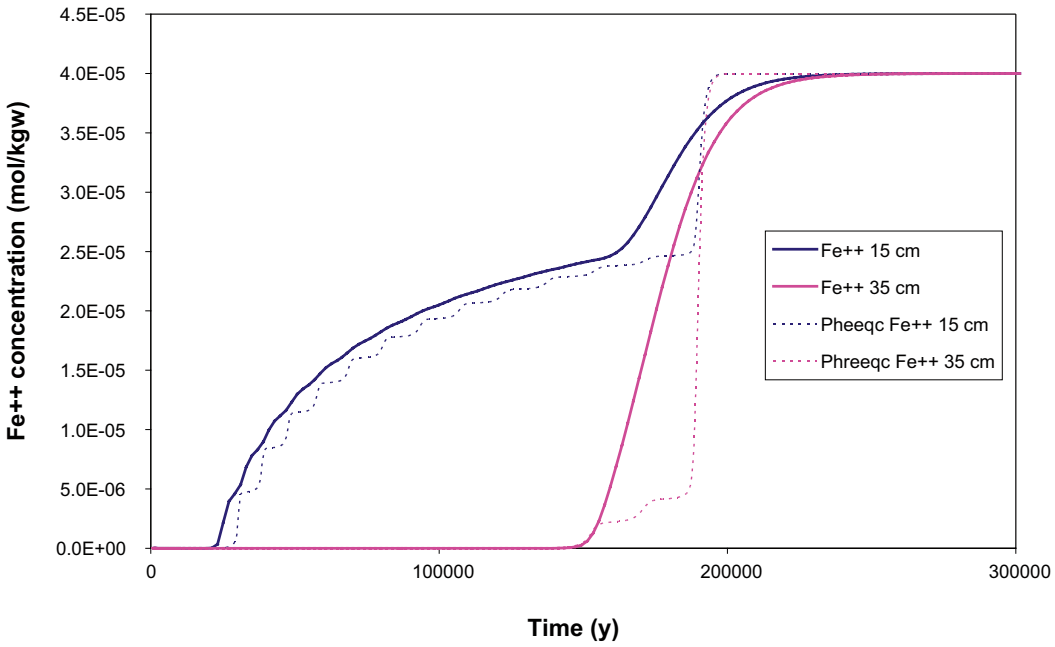

Figure 3-5. *Comparison of CrunchFlow and Phreeqc results of case B from Section 3.3.2.*

Case C0: Figure 3-6 shows the resulting mineral distributions after 100,000 and 500,000 years, respectively. From this picture, it is apparent that montmorillonite is slowly being dissolved but that only very small amounts of iron-rich clay phases are precipitating (berthierine). Almost all of the incoming iron is precipitated as magnetite. As illustrated in Figure 3-7, the pH value shows a minor increase near the Fe source, which is related to the depletion of montmorillonite in this zone. Fe(II) concentrations are calculated to remain low throughout the buffer (Figure 3-7).

Case C1: Excluding magnetite precipitation leads to a much larger clay conversion as the major part of the incoming iron in this case is available for montmorillonite-to-berthierine transformation. Still, as can be seen in Figure 3-8, only the first few centimetres are affected even after 500,000 years of conversion. Figure 3-9 shows the water chemistry evolution. The step-like behaviour seen for the iron concentration at 3 cm is due to the successive montmorillonite depletion in the cells closest to the Fe source.

The dissolution of montmorillonite is also seen in Figure 3-10, where the sorbed iron concentration at different positions is plotted as a function of time. The linear decreases seen at 1, 3 and 5 cm are due to dissolution of montmorillonite and hence loss of sorption sites. Note that the Fe sorption concentration is very small everywhere as most of the incoming iron is precipitated as berthierine.

Case C2: The porosity update switch for test case C1 was turned off in order to study the effect of a constant porosity throughout the calculation, independent of the precipitation/dissolution processes. The result is presented in Figure 3-11. Qualitatively, almost no change is noted with regard to test case C1 (compare Figure 3-11 with Figure 3-8) indicating that clogging effects are not significant. The porosity is increased by about 10% by the montmorillonite-to-berthierine conversion.

Case C3: This case is identical to C0 except that the diffusion coefficient was increased by an order of magnitude. In this situation, a clear clogging effect is noted (Figure 3-12) due to magnetite precipitation and the more rapid Fe mass transfer – the inlet is clogged after 100,000 years, which prevents further reactions from occurring.

Case C4: The montmorillonite solubility was raised by changing the log K of its dissolution reaction (Table 3-6) to a value of 15.0. In other respects, this case is identical to C0. In this case, the diffusive flow of silica out of the system becomes larger resulting in a more enhanced berthierine precipitation at the vicinity of the Fe source. This induces a clogging effect which slows down the conversion process at long times (Figure 3-13).

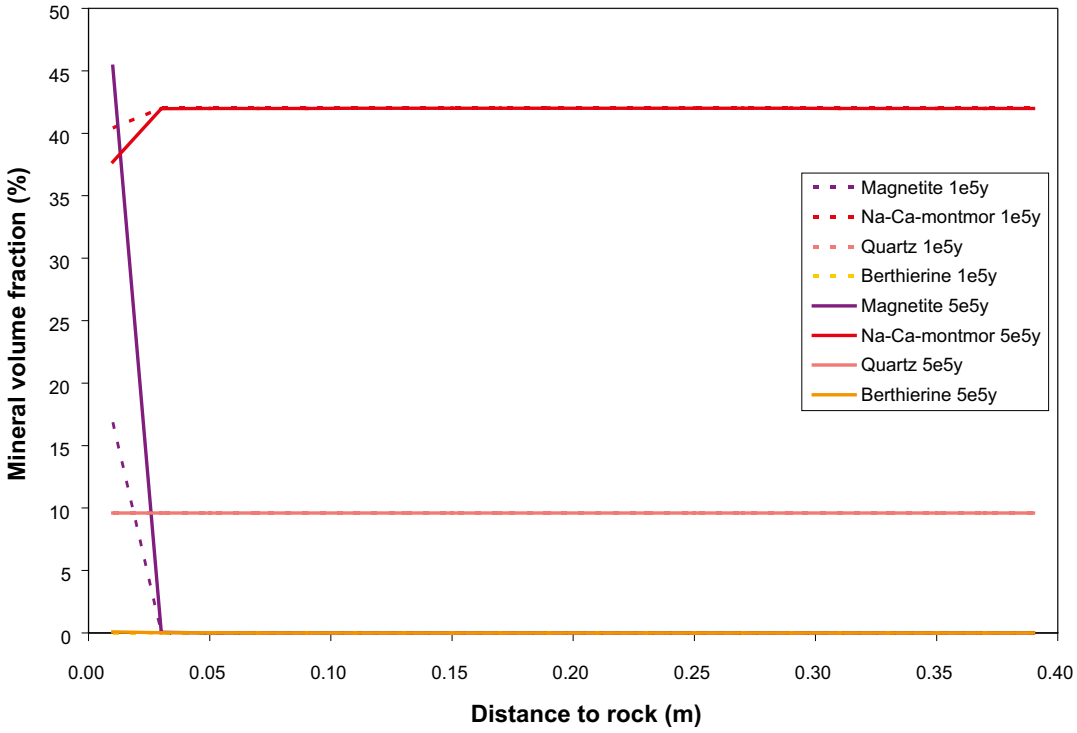

Figure 3-6. *Mineral distribution case C0 for $5 \cdot 10^5$ years (solid lines) and 10^5 years (hatched lines) Magnetite precipitation included.*

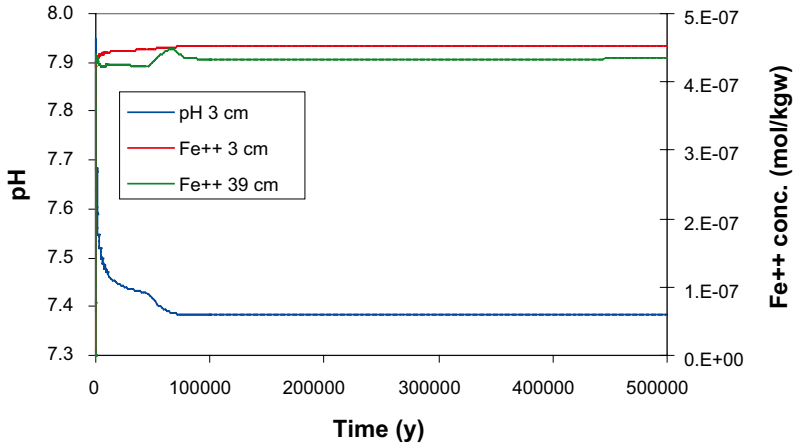

Figure 3-7. *pH evolution and dissolved iron concentration for test case C0.*

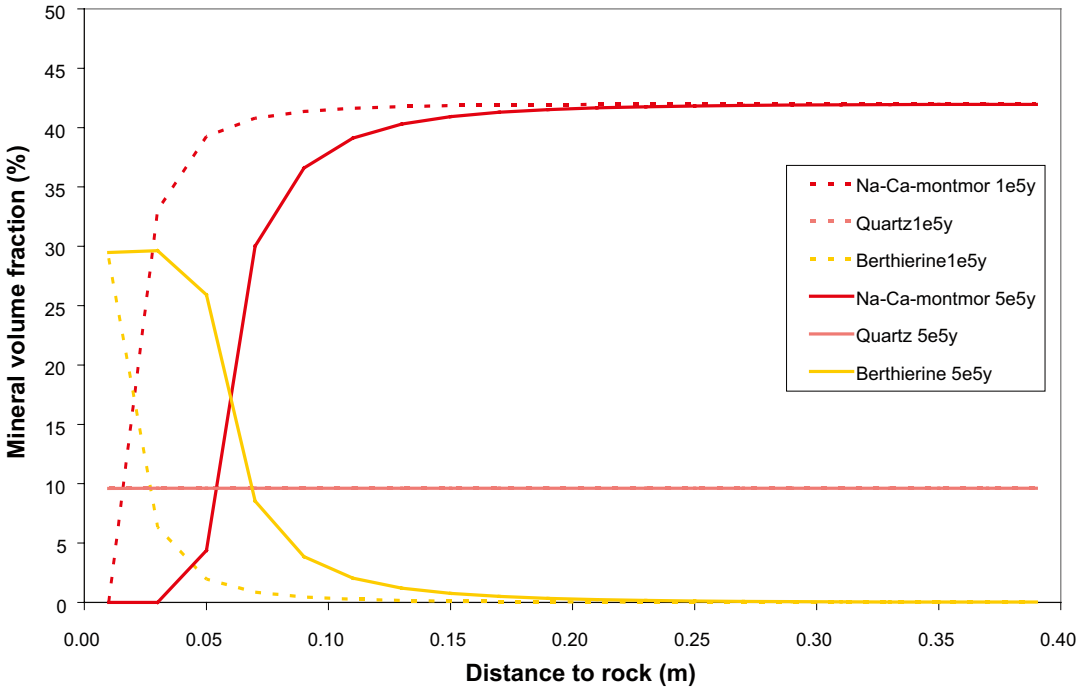

Figure 3-8. *Mineral distribution case C1 for $5 \cdot 10^5$ and 10^5 years. Magnetite precipitation excluded.*

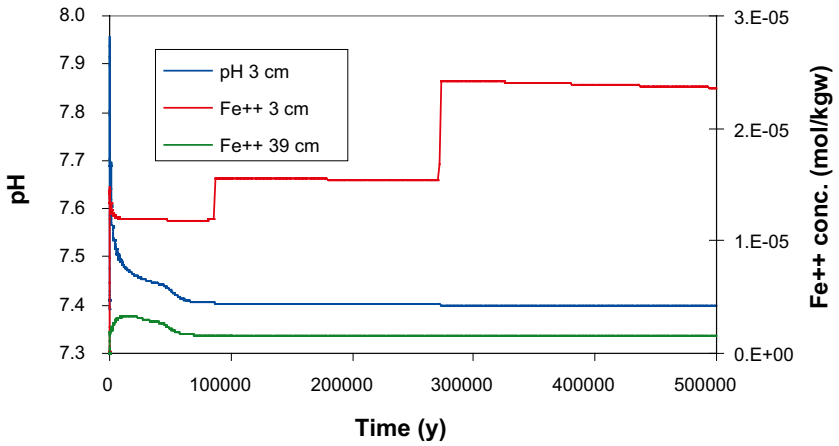

Figure 3-9. *pH and Fe(II) concentration for test case C1.*

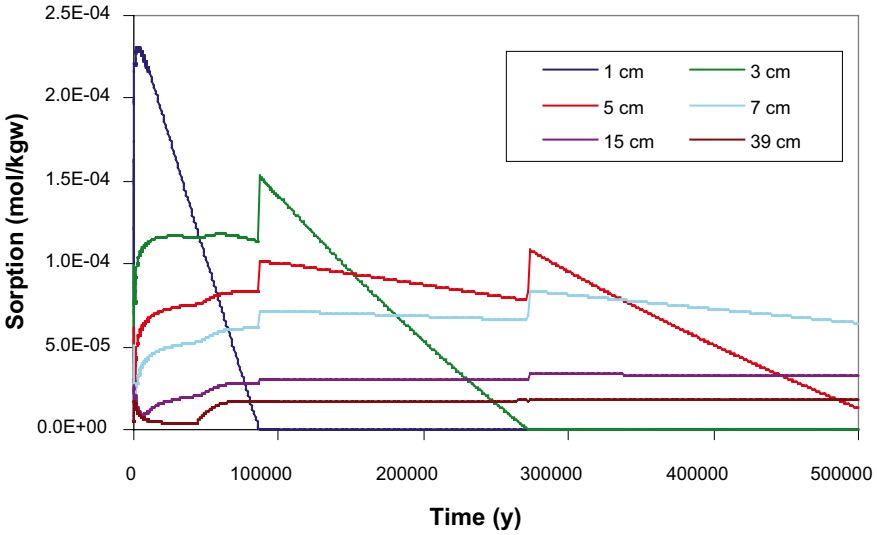

Figure 3-10. *Evolution of sorbed Fe concentrations at different positions in the buffer for test case C1.*

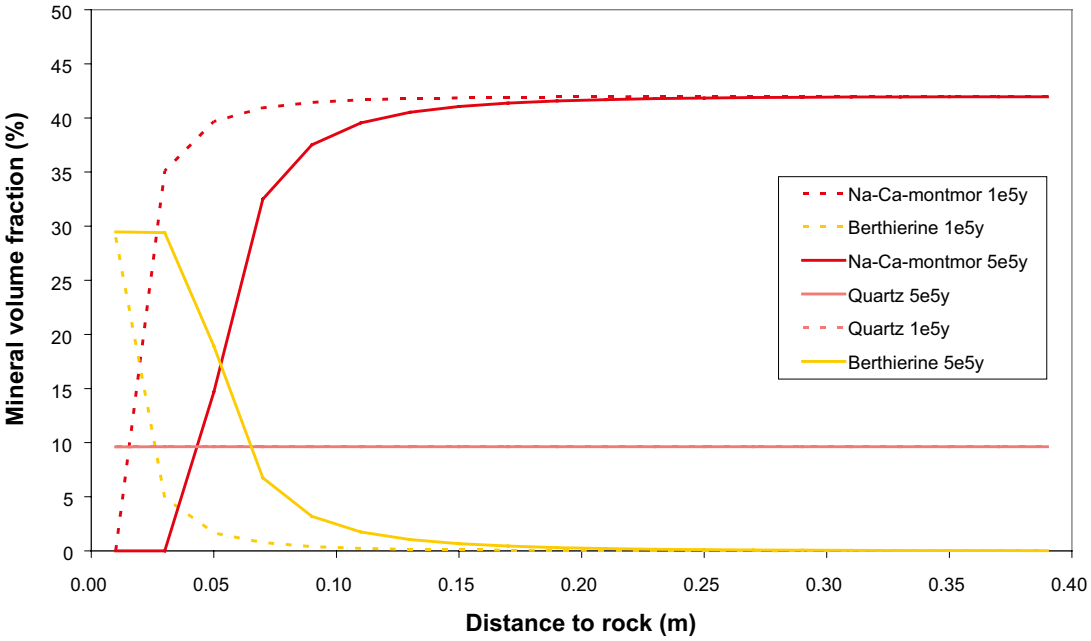

Figure 3-11. *Mineral distribution case C2 for $5 \cdot 10^5$ and 10^5 years. Magnetite precipitation excluded.*

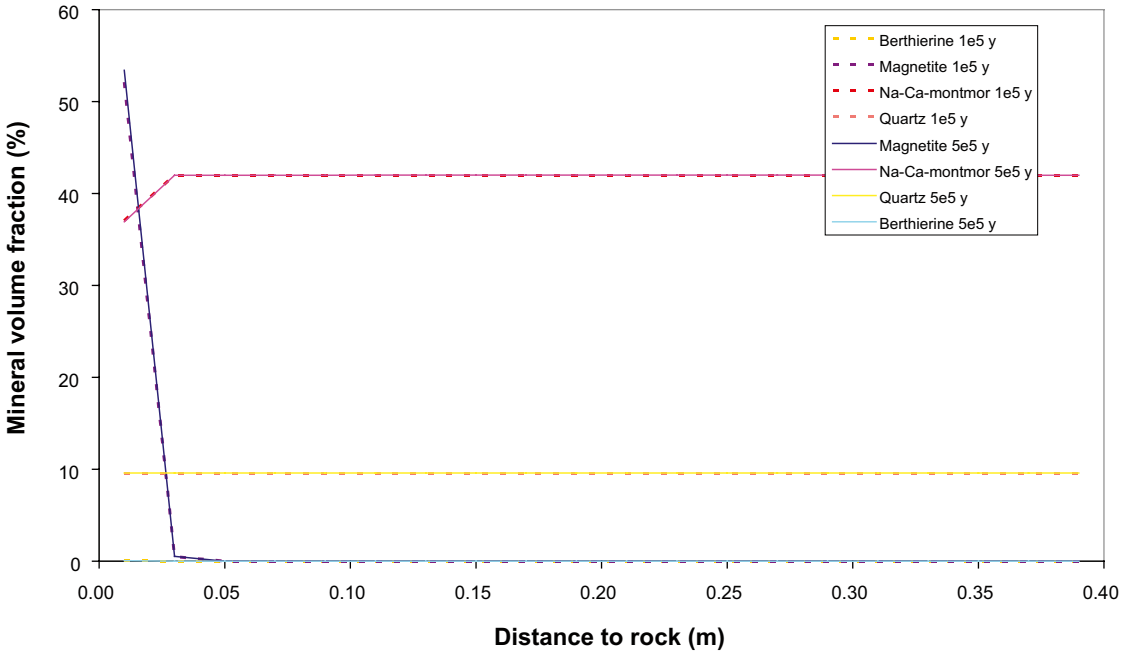

Figure 3-12. *Mineral distribution for test case C3 for $5 \cdot 10^5$ years (solid lines) and 10^5 year (hatched lines). Magnetite precipitation included, higher diffusion coefficient.*

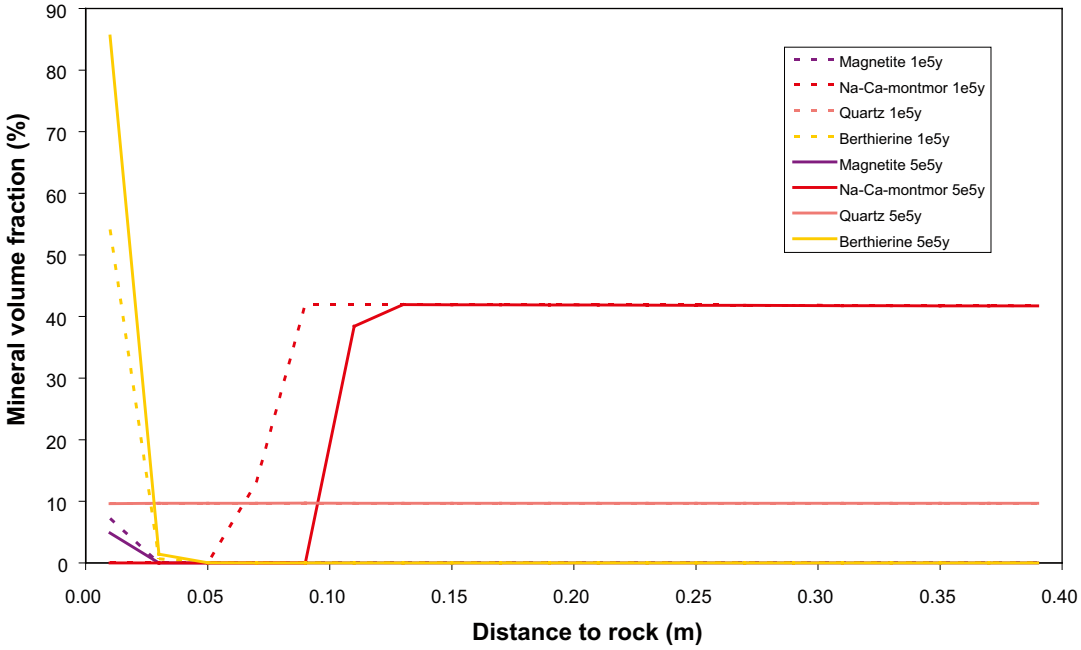

Figure 3-13. *Mineral distribution for test case C4 for $5 \cdot 10^5$ years and 10^5 years. Magnetite precipitation included, higher montmorillonite solubility.*

Test Case D

Treatment of corrosion reactions

For test case D, the SC corrosion reaction was specifically included. A uniform zero-order corrosion rate of 1 µm/a was assumed. With a steel thickness of 8 mm, complete corrosion of the SC will thus take 4,000 years (see also Section 2.5.1). By dividing by the molar volume of iron, 7.11×10^{-6} m^3/mol, and using 1 y = 3.15×10^7 s the corrosion rate can be expressed as

$k_{Iron}^{T_0} = 4.46 \cdot 10^{-6}$ mol m^{-2} s^{-1}.

When treating corrosion explicitly, an amount of iron corresponding to the correct iron-to-bentonite mass ratio in the KBS-3H concept (approximately 5.3%) is introduced in the model. The rate expression in CrunchFlow is:

$$Rate = \frac{dm}{dt} = s_{Iron} \cdot m \cdot k_{Iron}^{T_0} \qquad \text{(Equation 3-9)}$$

Where s_{Iron} is the specific surface area of the iron (m^2/g). As the CrunchFlow rate expression depends on the mass of iron present (first order expression), it is not possible to obtain a constant corrosion rate but the mass will decrease exponentially. In the present case, a specific surface area has been chosen in order to have lost most of the metallic iron after 4,000 years. The mass loss of iron as a function of time is illustrated in Figure 3-14.

When including corrosion in the reactive transport scheme explicitly, the model becomes more complex. It is now neccesary to handle not only the iron-buffer interface, but also the interface between iron and host rock. Since this study is primarily aimed at investigating the chemical response of bentonite we have chosen a more symmetric model where the host rock is replaced by bentonite and the amount of iron is increased in order to maintain the correct iron/bentonite mass ratio. The geometry used in this is depicted in Figure 3-15. Iron is corroded in a cell in the middle of the modelled area, a bentonite buffer similar in constitution to what has been used in the previous test cases is put on both sides of the corrding iron cell. To the left of the outer bentonite a boundary condition, identical to that used in the previous simulations, was imposed. Notice that the size of the iron cell is not related to the physical dimensions of the SC, but instead represents the discretisation region in the present model. The amount of iron in this cell, however, is chosen to get the same iron/bentonite ratio in the model as in the KBS-3H concept (see Figure 3-14).

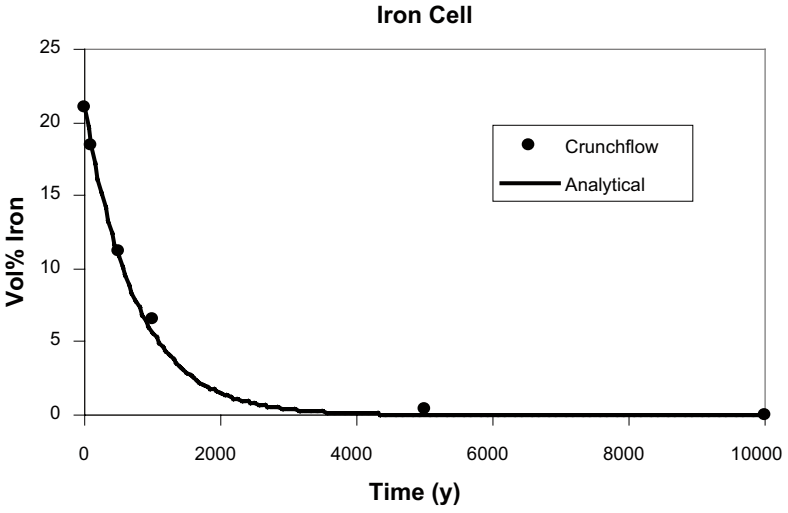

Figure 3-14. *Iron corrosion rate as used in the model (see text).*

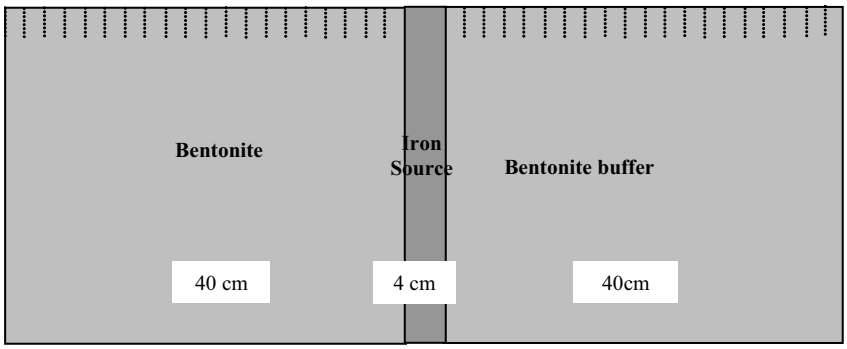

Figure 3-15. *Model geometry used for test case D (for explanation see text).*

The model

Case D0: Similar to case C0, magnetite is allowed to precipitate. Also cronstedtite, berthierine, FeS(am), quartz and siderite are considered as well as the initially present minerals. Fe(II) sorption is included. Distribution of minerals in the buffer after 100,000 years is illustrated in Figure 3-16. Similar to test cases C, it is seen that only the outer part is influenced. Most of the corroding iron has precipitated as clay phases and magnetite. In contrast to the C cases, calcite is still present in the buffer after 100,000 years. This is because of the higher pH values during the corrosion phase in this simulation.

The evolution of pH and Fe(II) concentration is shown in Figure 3-17. The pH-peak seen for a point 3 cm inside the buffer at the beginning of the simulation is due to the corroding iron. The Fe(II) concentration in the buffer is low at all times as the corroded iron either has precipitated or sorbed.

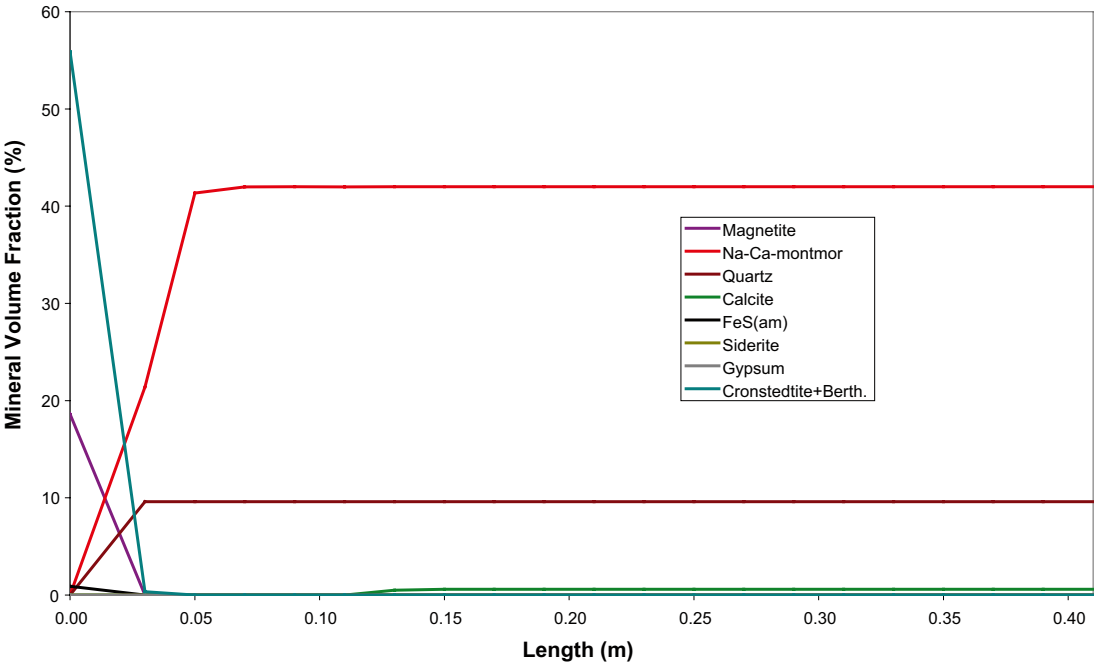

Figure 3-16. *Mineral distribution for case D0 for 10^5 years. Corrosion is explicitly included. Length means here distance to (centre of) iron source.*

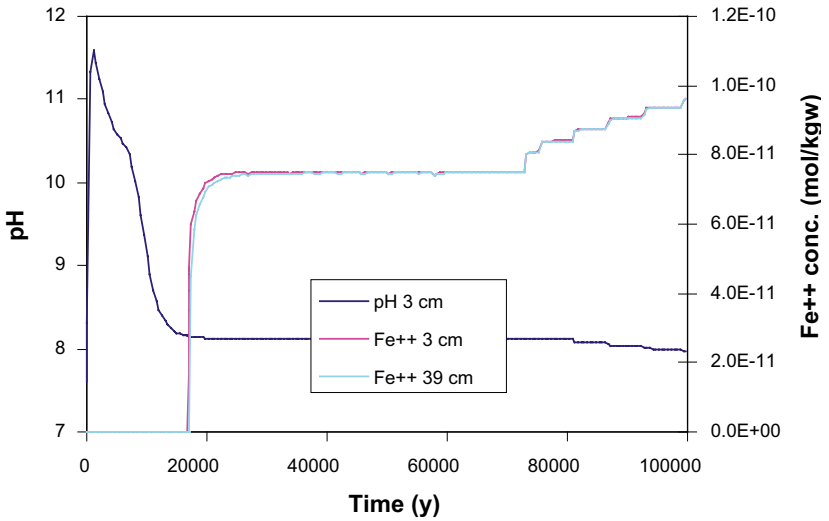

Figure 3-17. *Evolution of pH and Fe(II) for test case D0.*

3.3.4 Discussion

The geochemical modelling approach presented above is based on thermodynamic, kinetic and diffusion data, which partly display rather high uncertainties and thus the results for Fe transport and clay transformation processes should be regarded with care. Nevertheless, the coupling of equilibrium, kinetic and mass transport helps greatly to constrain the studied key processes and their evolution within the buffer. Overall, the modelling data indicate the spatially limited extent of the buffer affected by iron-bentonite interactions, even after very long time periods. This is mainly due to the low Fe(II) gradient between the source and the buffer, the strong sorption of Fe(II) to the clay and the Fe precipitation reaction leading to partial clogging. There are several parameters and inherent assumptions in the applied geochemical model that deserve some discussion with regard to their uncertainty and influence on the results:

Fe source concentration: This parameter will obviously have a significant affect on the Fe flux from the source – via Fick's law – and the resulting iron-bentonite interaction processes. In the test cases, two different scenarios were considered. In the constant Fe(II) scenario, it is implicitly assumed that corrosion and Fe transport are decoupled, on the basis that corrosion is estimated to occur rather fast for the time of interest. Thus, this scenario represents a pessimistic bounding case. Also, because of the constant flux of "fresh" groundwater, the porewater geochemistry is conditioned by that of the groundwater, thus limiting temporal geochemical variations. By explicitly introducing the corrosion process scenario, no large differences with regard to Fe fluxes or clay reaction products are predicted. This arises because of the rather fast corrosion rate relative to diffusion-reaction processes. However, water chemistry changes occur, resulting in an increase in pH, which are principally because of the treatment as closed system (as outlined above). Hence, this treatment can be regarded as further limiting case, in which very little water exchange with the host rock occurs over time.

Groundwater geochemistry: The long-term groundwater composition at Olkiluoto which will control the Fe(II) solubility and sorption is quite uncertain. The possible variations have been considered by analysing geochemical information and deriving a "realistic" test case A with moderately saline conditions and a rather extreme upper case representing a mixture of saline and meteoric groundwater. The latter scenario was assumed for all other test cases, in order to obtain conservative estimates of Fe fluxes and resulting iron-bentonite interaction processes. Therefore the possible variability of groundwater conditions that affect Fe-clay interaction is reasonably well represented in the model. It is important to note that upconing of deep saline water is expected to result in low Fe(II) concentrations (cf. Table 3-2), and hence the impact is expected to be comparable to the "realistic" case.

Diffusion process: Diffusion through the compacted bentonite buffer is treated in the model in (overly) simplistic fashion, by considering a uniform diffusion coefficient and porosity for all species. The effective diffusion coefficient is thus assumed to be an average value for cations and anions, which, however, are known to differ in compacted bentonite /e.g. Yu and Neretnieks 1997, Ochs et al. 2001/. Based on a rather extensive compilation of diffusion measurements, /Ochs and Talerico 2004/ recommended average D_e values for anions of 10^{-11} m^2/s (and porosities of 0.17) in the SR-Can assessment. For cations, considerably higher D_e values of 10^{-10} m^2/s were recommended (and porosities of 0.43), which, according to the authors, should account for an additional driving force for diffusion in the electric double layer. This significant difference in diffusion coefficients between cations and anions highlights the difficulty of applying consistent diffusion data in reactive transport modelling. Effects of the electric double layer of the charged clay surface or of multicomponent diffusion are not accounted for due to current lack of understanding.

The applied effective diffusivity coefficient of 2×10^{-11} m^2/s is similar to that used in previous reactive transport studies in the bentonite buffer /e.g. Gaucher et al. 2004/. The use of a D_e of 10^{-10} m^2/s instead of 2×10^{-11} m^2/s leads to more rapid breakthrough of the Fe(II) sorption front by a factor of five, thus in the "dilute groundwater scenario" (test case B) the breakthrough at the centre of the buffer would be reduced to 30,000 years. It is important to note that Fe(II) sorption alone does not affect the buffer's integrity and that even for a high Fe(II) diffusion coefficient, the extent of affected buffer will probably not be large. This is indicated from reactive transport calculations with higher D_e, where neo-formation of Fe phases is still limited to a few cm after 500,000 years, mainly due to clogging effects.

A further simplification is the assumption of linear instead of radial geometry. This, however, is not expected to strongly affect the results. In fact, a slight decrease in the Fe(II) movement is expected due to the general more rapid evening of the concentration gradients.

Fe(II) sorption: In the model, sorption is described via surface complexation to edge sites and cation exchange to interlayer sites, based primarily on the PhD thesis of /Tournassat 2003/. This work and also later studies performed in the same research group indicate a more complex Fe(II) uptake process at pH > 7, namely a coupled redox/precipitation reaction. The exact mechanism still being unclear, it has been suggested by /Charlet 2006/ that Fe(II) uptake at the smectite surface occurred as co-precipitation of a an Fe-rich clay rather than as an adsorption process. Relating this hypothesis to our case study, this would considerably retard the movement of Fe(II) into the buffer relative to (reversible) surface sorption, as assumed in our model.

The sorbed iron front, may, in principle, affect sorption of radionuclides by competition effects once the canister is corroded. This aspect has not been studied in detail, as outlined in Section 2.2, and thus considerable uncertainty remains. On the other hand, our reactive transport calculations indicate a strong retardation of the Fe(II) sorption front due to precipitation phenomena.

Comparison to other modelling studies: It is noteworthy that two other modelling exercises /Fritz et al. 2006, Bildstein et al. 2006/ dealing with the interaction of corrosion-derived Fe and bentonite in the EBS, also illustrate the important diffusional constraint of Fe (see Section 2.3.4). In both studies, clay transformation reactions are taken into account, but no sorption reactions. According to the both modelling results, the interaction of Fe with bentonite remains spatially limited for very long times mainly because of Fe clay re-precipitation and diffusional limitation.

4 Conclusions and recommendations

Steel components are unstable in EBS environments. They will corrode to fairly insoluble corrosion products, such as magnetite, and also react with the smectitic matrix. The extent of the interaction of reduced Fe with smectite under repository relevant conditions is not well known because of insufficient experimental and natural analogue information. In spite of this drawback, qualitative and quantitative considerations on the impact of steel components on the performance of the buffer can be made with the help of experimental data in the literature and design and site-specific information.

Montmorillonite may incorporate only a limited amount of Fe, mainly as Fe(III), in its structure. Fe(II) derived from the corrosion process will strongly interact with the montmorillonite surface by sorption and, for non-acidic conditions, presumably also by redox and surface precipitation reactions. Under very reducing conditions, it may also reduce structural Fe(III), which would destabilise the montmorillonite structure.

The interaction of Fe with bentonite will also induce slow transformation of montmorillonite via dissolution and re-precipitation of a Fe^{2+}-rich clay. The kinetics and pathways of this reaction are still poorly known. Moreover, the extent of this reaction will be affected by mass transfer constraints of Fe^{2+} in a diffusive system (analogous to K^+ in the illitisation reaction). The most likely reaction products under repository conditions are Fe-rich smectite (e.g. Fe-saponite), berthierine or chlorite.

Effects of iron-bentonite interaction on the buffer's physical properties have been even less studied than effects on geochemical ones. In principle, both smectite transformation and cementation may result in reduced buffer performance. A preliminary study /Carlson et al. 2006/ suggests that swelling properties may be much less affected than hydraulic conductivity by the interaction process. The reason for the observed hydraulic conductivity increase in that study remained however unclear. Cementation by precipitation of iron oxides is likely to occur under oxic conditions, as also suggested by observations from natural systems. Under anoxic conditions, natural analogue examples are lacking to our knowledge that would indicate any effects of cementation resulting from Fe(II) precipitates.

A preliminary assessment on the impact of Fe on the buffer for the KBS-3H concept, using the Olkiluoto site as a test case, was carried out. A simple mass balance estimate indicates that substantial amounts of montmorillonite (10–30%) would be transformed if all the iron from the supercontainer steel shell would react with it and produce a non-swelling Fe clay. This would induce a decrease in swelling pressure from 7 to 2 MPa. However, there are several factors that will limit the extent of Fe-clay interaction. First, the precipitation of insoluble iron phases (magnetite, FeS_{1-2} and perhaps siderite) will compete for Fe. Second, transport of Fe is limited by diffusion. Third, the diffusive flux of Fe(II) into the buffer, which depends on the concentration gradient of Fe(II) between the corroded source and the buffer, is expected to be small. Moreover, this gradient will be effectively lowered at the reaction front by the strong interaction of dissolved Fe(II) with the clay.

Hence, a more realistic (but still rather simple) reactive transport model with aid of the Phreeqc and CrunchFlow codes was performed. Both Fe(II) sorption and precipitation as well as montmorillonite transformation were assessed by a number of test case calculations. These modelling results indicate that the flux of Fe into the buffer will be small and the extent of the buffer zone affected by iron-bentonite interaction processes will be limited. The largest Fe flux would arise from a relatively soluble $FeCO_3$ source and concomitant low Fe(II) activity in the porewater of the unaffected buffer. But even for this case and time scales of 10^5 years, no large detrimental effect on the buffer were predicted. It should be noted that the uncertainties in the underlying thermodynamic and kinetic data and in the description of solute diffusion are rather large.

In conclusion, this preliminary study indicates that for the KBS-3H design adverse effects on the swelling buffer material may occur due to interaction between the supercontainer iron and bentonite, but that these will be spatially limited to the outermost few cm near the buffer-supercontainer steel shell-rock interface for very long time periods. This physically affected area close to the supercontainer steel shell, consisting of corrosion products and transformed clay material, however needs to be considered in performance assessment calculations. Also the processes related to the interaction of iron on the buffer are complex and the consequent impact on the required properties of bentonite is far from being completely understood.

A final point to consider is the potential competition of Fe(II) with radionuclides for sorption sites, which, in principle, may weaken the sorption of the latter. Preliminary experimental data do not support such a competition effect, rather the opposite. Moreover, results from reactive transport calculations indicate that the Fe sorption front will not extend far into the buffer for very long times. The iron source zone may in fact act as efficient sink for radionuclides, in particular, for redox sensitive ones, such as uranium or selenium.

Recommendations:

From the experimental side, iron-bentonite interaction studies should include measurements of physical properties (swelling pressure, hydraulic conductivity). In such studies, it is critical to work at low Eh conditions to limit oxidation to Fe^{3+} and resulting cementation effects. The minimization of oxygen ingress however is a challenging task. A further route to follow is the conductance of well-controlled diffusion experiments with Fe(II). Furthermore, the potential effect of H_2 on Fe-clay interactions and on reduction of structural iron in smectite should be experimentally investigated.

From the modelling side, more advanced geochemical modelling, which includes cation and anion diffusion in rigorous manner, is a prerequisite for more realistic system description. This includes the inclusion of multicomponent diffusion effects and diffusion in the interlayer in reactive transport codes. Efforts to include such effects are in progress /e.g. Appelo and Wersin 2007/.

References

Aagard P, Helgeson H C, 1983. Activity/composition relations among silicates and aqueous solutions: II. Chemical and thermodynamic consequences of ideal mixing of atoms on homological sites in montmorillonites, illite and mixed-layer clays. Clays and Clay Minerals 31, 207–217.

Aagard P, Jahren J, Harstad A, Nilsen O, Ramm M, 2000. Formation of grain-coating chlorite in sandstones. Laboratory synthesized vs. natural occurrences. Clay Miner. 35, 261–269.

Ahokas H, Hellä P, Ahokas T, Hansen J, Koskinen K, Lehtinen A, Koskinen L, Löfman J, Mészáros F, Partamies S, Pitkänen P, Sievänen U, Marcos N, Snellman M, Vieno T, 2006. Control of water inflow and use of cement in ONKALO after penetration of fracture zone R19. Posiva Working Report 2006-45. Posiva Oy, Olkiluoto, Finland.

Andersson J, Ahokas H, Hudson J A, Koskinen L, Luukkonen A, Löfman J, Keto V, Pitkänen P, Mattila J, Ikonen A I T, Ylä-Mella M, 2007. Olkiluoto Site Description 2006, POSIVA 2007-03. Posiva Oy, Olkiluoto, Finland.

Andra, 2001. Materials Baseline Volume 4. Corrosion of metallic materials. Andra Report C.RP.AMAT.01.060, Châtenay-Malabry, France.

Andra, 2005. Dossier 2005: Référentiel des matériaux d'un stockage de déchets a haute activité et a vie longue. Tome 1: Matériaux à base d'argiles gonflantes. Andra report C.RP. ASCM.04.0015.A, Châtenay-Malabry, France.

Appelo C A J, Wersin P, 2007. Multicomponent diffusion modeling in clay systems with application to the diffusion of tritium, iodide and sodium in Opalinus Clay. Environ. Sci. Technol. 41, 5002–5007.

Autio J, Börgesson L, Sandén T, Rönnqvist P-E, Berghäll J, Kotola R, Parkkinen I, Johansson E, Hagros A, Eriksson M, 2007. KBS-3H Design Description 2006. Posiva Working report 2007-105. Posiva Oy, Olkiluoto, Finland. Svensk Kärnbränslehantering AB.

Badaut D, Besson G, Decarreau A, Rautureau R, 1985. Occurrence of a ferrous, trioctahedral smectite in Recent sediments of Atlantis II Deep, Red Sea. Clay Minerals 20, 389–404.

Baeyens B, Bradbury M H, 1997. A mechanistic description of Ni and Zn sorption on Na-montmorillonite. Part I: Titration and sorption measurements. J. Contam. Hydrology 27, 199–222.

Berner R A, 1980. Early diagenesis: A theoretical approach. Princeton University Press, 241 pp.

Bildstein O, Trotignon L, Hairapetian T, Jullien M, 2006. Modelling iron corrosion in clayey environments: implications for the near field geochemistry in HLW repositories. In Wersin P. & Mettler S. 2006. Workshop on Fe-clay interactions in repository environments, a joint initiative by Andra, SKB and Nagra. Basel 9–10 May 2006. NAB-06-15. Nagra, Wettingen, Switzerland.

Bradbury M H, Baeyens B, 1997. A mechanistic description of Ni and Zn sorption on Na-montmorillonite. J. Contam. Hydrol. 27, 223–248.

Bradbury M H, Bayens B, 2002. Porewater chemistry in compacted re-saturated MX-80 bentonite: physico-chemical characterisation and geochemical modelling. Nagra Technical Report NTB 01-08, Wettingen, Switzerland.

Bruno J, Arcos D, Duro L, 1999. Processes and features affecting the near field chemistry. Groundwater-bentonite interaction. SKB TR-99-29. Svensk Kärnbränslehantering AB.

Buatier M, Honnorez J, Ehret G, 1989. Fe-smectite-glauconite transition in hydrothermal green clays from the Galapagos spreading center. Clays and Clay Minerals 37, 532–541.

Börgesson L, Sandén T, Fälth B, Åkesson M, Lindgren E, 2005. Studies of buffers behavior in KBS-3H concept, Work during 2002–2004. R-05-50. Svensk Kärnbränslehantering AB.

Carlson L, Karnland O, Olsson S, Smart N, Rance A, 2006. Experimental studies on the interaction between anaerobically corroding iron and bentonite, Posiva Working Report 2006-60. Posiva Oy, Olkiluoto, Finland. Svensk Kärnbränslehantering AB.

Carstea D D, 1968. Formation of hydroxy-Al and -Fe interlayers in montmorillonite and vermiculite: Influence of particle size and temperature. Clays and Clay Minerals 16, 231–238.

Carstea D D, Harward M E, Knox E G, 1970. Comparison of iron and aluminum hydroxy interlayers in montmorillonite and vermiculite: I. formation. Soil Sci. Soc. Amer. Proc. 34, 517–521.

Cathelineau M, Izquierdo G, 1988. Temperature-composition relationships of authigenic micaceous minerals in the Los Azufres geothermal system. Contrib. Mineral. Petrol. 100, 418–428.

Cathelinau M, Guillaume D, Mosser-Ruck R, Dubessy J, Charpentier D, Villiéras F, Michau N, 2005. Dissolution-crystallization processes affecting dioctahedral smectite in the presence of iron: implication on mineral distribution in clay barriers, ANDRA International Conference, 14–18 March 2005, Tours, France.

Charlet L, Tournassat C, 2005. Fe(II)-Na(I)-Ca(II) cation exchange on montmorillonite in chloride medium: evidence for preferential clay adsorption of ions pairs in marine environment chemical modelling and XRD profile modelling study. Aquatic Geochemistry 11, 115–137.

Charlet L, 2006. Transfers through the reactive clay barriers in radioactive waste repositories. Surface reactions between Fe^{2+} and smectites. In Wersin P. & Mettler S. 2006. Workshop on Fe-clay interactions in repository environments, a joint initiative by Andra, SKB and Nagra. Basel 9–10 May 2006. NAB-06-15. Nagra, Wettingen, Switzerland.

Chermak J A, Rimstidt J D, 1989. Estimating the thermodynamic properties of silicate minerals at 298 K from the sum of polyhedral contributions. American Mineralogist 74, 1023–1031.

Christidis G E, Scott P W, 1997. The origin and control of colour of white bentonites from the Aegean islands of Milos and Kimolos. Mineralium Deposita 32, 271–279.

Curti E, Wersin P, 2002. Assessment of porewater chemistry in the bentonite backfill for the Swiss SF/HLW repository. Nagra Technical Report NTB 02-09, Nagra, Wettingen, Switzerland.

David D, 2001. Analogues archéologiques et corrosion. Andra Report, Chatenay-Malabry, France.

Dixon D A, 2000. Porewater salinity and the development of swelling pressure and bentonite-based buffer and backfill materials. POSIVA 2000-04. Posiva Oy, Helsinki, Finland.

Dong H, Fredrickson J K, Kennedy D W, Zachara J M, Kukkadapu R K, Onstott T C, 2000. Mineral transformation associated with the microbial reduction of magnetite. Chem. Geol. 169, 299–318.

Drits V A, Manceau A, 2000. A model for the mechanism of Fe^{3+} to Fe^{2+} reduction in dioctahedral smectites. Clays and Clay Minerals 48, 185–195.

Foster M D, 1953. Geochemical studies of clay minerals: II. Relation between ionic substitution and swelling in montmorillonites. Amer. Mineral. 38, 994–1006.

Fritz B, Marty N, Clément A, Michau N, 2006. Geochemical modelling of the influence of iron corrosion on bentonite stability. In Wersin P. & Mettler S. 2006. Workshop on Fe-clay interactions in repository environments, a joint initiative by Andra, SKB and Nagra. Basel 9–10 May 2006. NAB-06-15. Nagra, Wettingen, Switzerland.

Gallahan W E, Duncan R A, 1994. Spatial and temporal variability in crystallization of celadonites within the Troodos ophiolite, Cyprus: Implications for low-temperature alteration of the oceanic crust. J. Geophysical Research 99, 3147–3162.

Gaucher E, Blanc P, Matray J-M, Michau N, 2004. Modeling diffusion of an alkaline plume in a clay barrier, Applied Geochemistry 19, 1505–1515.

Génin J-M R, Bourrié G, Trolard F, Abdelmoula M, Jafreciz A, Refait P, Maitre V, Humbert B, Herbillon A, 1998. Thermodynamic equilibria in aqueous suspensions of synthetic and natural Fe(II)-Fe(III) green rusts: Occurrences of the mineral in hydromorphic soils. Environ. Sci. Technol. 32, 1058–1068.

Gérard F, Clement A, Fritz B, 1998. Numerical validation of a Eulerian hydrochemical code using a 1D multisolute mass transport system involving heterogeneous kinetically controlled reactions. J. Contam. Hydrol. 30, 201–216.

Gerstl Z, Banin A, 1980. Fe^{2+}-Fe^{3+} transformations in clay and resin ion-exchange systems. Clays and Clay Minerals 28, 335–345.

Guillaume D, 2002. Etude expérimentale du système fer-smectite en présence de solution à 80°C et 300°C. PhD thesis, University Henri Poincaré, Nancy I, France.

Guillaume D, Neaman A, Cathelineau M, Mosser-Ruck R, Pfeiffert C, Abdeloula M, Dubessy J, Villéras F, Baronnet A, Michau N, 2003. Experimental synthesis of chlorite from smectite at 300°C in the presence of metallic Fe. Clay Minerals 38, 281–302.

Guillaume D, Neaman A, Cathelineau M, Mosser-Ruck R, Pfeiffert C, Abdelmoula M, Dubessy J, Villiéras F, Michau N, 2004. Experimental study of the transformation of smectite at 80 and 300°C in the presence of Fe oxides. Clay Minerals 39, 17–34.

Güven N, 1988. Smectites. In Hydrous Phyllosilicates, S.W. Bailey (ed.), Reviews in Mineralogy, Vol. 19, Mineralogical Society of America, pp. 497–559.

Habert B, 2000. Réactivité du fer dans les gels et les smectites. PhD thesis, University of Paris 6, France.

Haveman S A, Pedersen K, Ruotsalainen P, 1998. Geomicrobial investigations of groundwater from Olkiluoto, Hästholmen, Kivetty and Romuvaraa, Finland. POSIVA 98-09. Posiva Oy, Helsinki, Finland.

Haveman S A, Larsdotter Nilsson E, Pedersen K, 2000. Regional distribution of microbes in groundwater from Hästholmen, Kivetty, Olkiluoto and Romuvaara, Finland. POSIVA 2000-16. Posiva Oy, Helsinki, Finland.

Heller-Kallai L, 1997. Reduction and reoxidation of nontronite: the data reassessed. Clays and Clay Minerals 45, 476–479.

Hermansson H-P, 2004. The stability of magnetite and its significance as a passivating film in the repository environment. SKI Report 2004:07. SKI, Stockholm, Sweden.

Iijima A, Matsumoto R, 1982. Berthierine and chamosite in coal measures of Japan. Clays and Clay Minerals 30, 264-274.

Ikonen K, 2003. Thermal Analyses of KBS-3H Type Repository, POSIVA 2003-11. Posiva Oy, Olkiluoto, Finland.

JNC, 2000. H12: Project to establish the scientific and technical basis for HLW disposal in Japan. Supporting Report 2. Repository design and engineering technology. JNC TN1410 2000-003, Japan Nuclear Cycle Development Institute, Tokai, Japan.

Johnson L H, King F, 2003. Canister options for the disposal of spent fuel. Nagra Technical Report NTB 02-11. Nagra, Wettingen, Switzerland.

Johnson L, Marschall P, Wersin P, Gribi P, 2005. HMCBG processes related to the steel components in the KBS-3H disposal concept. Posiva Working Report 2005-09 and SKB R-08-25. Posiva Oy, Olkiluoto, Finland. Svensk Kärnbränslehantering AB.

Karnland O, Birgersson M, 2006. Montmorillonite stability with special respect to KBS-3 conditions. SKB TR-06-11. Svensk Kärnbränslehantering AB.

King F, Ahonen L, Taxén C, Vuorinen U, Werme L, 2001/2002. Copper corrosion under expected conditions in a deep repository. SKB TR-01-23. Svensk Kärnbränslehantering AB, Stockholm, Sweden, also POSIVA 2002-01. Posiva Oy, Helsinki, Finland.

Kostka J E, Nealson K H, 1995. Dissolution and reduction of magnetite by bacteria. Environ. Sci. Technol. 29, 2535–2540.

Kostka J E, Stucki J W, Nealson K H, Wu J, 1996. Reduction of structural Fe(III) in smectite by a pure culture of the Fe-reducing bacterium Shewanella putrifaciens strain MR-1. Clays and Clay Minerals, 44, 522–529.

Kostka J E, Wu J, Nealson K H, Stucki J W, 1999. The impact of structural Fe(III) reduction by bacteria on the surface chemistry of smectite clay minerals. Geochim. Cosmochim. Acta 63, 3705–3173.

Lanson B, 2006. Transformation processes of smectite in contact with metal iron: Mechanisms of smectite destabilization and characterization of the newly-formed phases. In Wersin P. & Mettler S. 2006. Workshop on Fe-clay interactions in repository environments, a joint initiative by Andra, SKB and Nagra. Basel 9–10 May 2006. NAB-06-15. Nagra, Wettingen, Switzerland.

Lantenois S, 2002. Iron-clay interaction in aqueous solutions. International Meeting, Clays in Natural and Engineered Barriers for Radioactive Confinement. December 9–12, 2002, Reims, France, O-10b-3.

Lantenois S, 2003. Réactivité fer métal/smectites en milieu hydraté à 80°C. PhD thesis, University of Orléans, France.

Lasaga A C, 1998. Kinetic Theory in the Earth Sciences, Princeton Univ. Press, Princeton, N.J.

Löfman J, Mészáros F, 2005. Simulation of hydraulic disturbances caused by the underground rock characterization facility in Olkiluoto, Finland. POSIVA 2005-08. Posiva Oy, Olkiluoto, Finland.

Madsen F T, 1998. Clay mineralogical investigations related to nuclear waste disposal. Clay Minerals 33, 109–129.

Marcos N, 2003. Bentonite-iron interactions in natural occurrences and in laboratory – the effects of the interaction on the properties of bentonite: a literature survey. Posiva Working Report 2003-55. Posiva Oy, Olkiluoto, Finland.

Mata M P, Giorgetti G, Árkai P, Peacor D R, 2001. Comparison of evolution of trioctahedral chlorite/berthierine/smectite in coeval metabasites and metapelites from diagenetic to epizonal grades. Clays and Clay Minerals 49, 318–332.

Mattigod S V, Sposito G, 1978. Improved method for estimating the standard free energies of formation ($\Delta G_{f,298.15}$) of smectites. Geochim. Cosmochim. Acta 42, 1753–1762.

May H M, Kinniburgh D G, Helmke P A, Jackson M L, 1986. Aqueous dissolution, solubilities, and thermodynamic stabilities of common aluminosilicate clay minerals: Kaolinite and smectites. Geochim. Cosmochim. Acta 50, 1667–1677.

Meunier A, 2005. Clays. Springer Verlag, 472 pp.

Müller-Vonmoos M, Kahr G, 1983. Mineralogische Untersuchungen von Wyoming Bentonit MX-80 und Montigel. Nagra Technical Report NTB 83-12. Nagra, Wettingen, Switzerland.

Müller-Vonmoos M, Kahr G, Bucher F, Madsen F, Mayor P-A, 1991. Untersuchungen zum Verhalten von Bentonit in Kontakt mit Magnetit und Eisen unter Endlagerbedingungen. Nagra Technical Report NTB 91-14. Nagra, Wettingen, Switzerland.

Muurinen A, Lehikonen J, 1999. Porewater chemistry in compacted bentonite. POSIVA 99-20. Posiva Oy, Helsinki, Finland.

Muurinen A, 2006. Chemical Conditions in the A2 Parcel of the Long-Term Test of Buffer Material in Äspö (LOT). Posiva Working Report 2006-83. Posiva Oy, Olkiluoto, Finland.

Nagra, 2002. Project Opalinus Clay: Safety report. Demonstration of disposal feasibility for spent fuel, vitrified high-level waste and long-lived intermediate-level waste (Entsorgungsnachweis). Nagra Technical Report NTB 02-05. Nagra, Wettingen, Switzerland.

Ochs M, Lothenbach B, Wanner H, Sato H, Yui M, 2001. An integrated sorption-diffusion model for the calculation of consistent distribution and diffusion coefficients in compacted bentonite. J. Contam. Hydrol. 47, 283–296.

Ochs M, Talerico C, 2004. SR-Can. Data and uncertainty assessment. Migration parameters for the bentonite buffer in the KBS-3 concept. SKB TR-04-18. Svensk Kärnbränslehantering AB.

Oscarson D W, Heimann R B, 1988. The effect of Fe(II)-silicate on selected properties of a montmorillonitic clay. Clay Minerals 23, 81–90.

Palandri J L, Kharaka Y K, 2004. A compilation of rate parameters of water-mineral interaction kinetics for application to geochemical modeling. U.S. Geological Survey Open File Report 2004-1068.

Parkhurst D L, Appelo C A J, 1999. User's guide to Phreeqc (Version 2) – A computer program for speciation, batch reaction, one-dimensional transport, and inverse geochemical calculations. U.S. Geological Survey Water-Resources Investigations Report 99-4259.

Pastina B, Hellä P, 2006. Expected evolution of a spent fuel repository at Olkiluoto. POSIVA 2006-05. Posiva Oy, Olkiluoto, Finland.

Pedersen K, 2000. Microbial processes in radioactive waste disposal. SKB TR-00-04. Svensk Kärnbränslehantering AB.

Pedersen K, 2006. Microbiology of Transitional Groundwater of the Porous Overburden and Underlying Fractured Bedrock Aquifers in Olkiluoto 2004, Finland. Posiva Working Report 2006-09. Posiva Oy, Olkiluoto, Finland.

Pedersen K, 2007. Microbiology of Transitional Groundwater of the Porous Overburden and Underlying Shallow Fractured Bedrock Aquifers in Olkiluoto, Finland, October 2005– January 2006, Finland. Posiva Working Report 2007-20. Posiva Oy, Olkiluoto, Finland.

Pitkänen P, Partamies S, Luukkonen A, 2004. Hydrogeochemical interpretation of baseline groundwater conditions at the Olkiluoto site. POSIVA 2003-07. Posiva Oy, Olkiluoto, Finland.

Pitkänen P, Ahokas H, Ylä-Mella M, Partamies S, Snellman M, Hellä P, 2007. Quality Review of Hydrogeochemical Baseline Data from the Olkiluoto Site, POSIVA 2007-05. Posiva Oy, Olkiluoto, Finland.

Posiva, 2003. Baseline conditions at Olkiluoto. POSIVA 2003-02. Posiva Oy, Olkiluoto, Finland.

Posiva, 2005. Olkiluoto Site Description 2004, Posiva Oy, Olkiluoto, Finland. POSIVA 2005-03. Posiva Oy, Olkiluoto, Finland.

Puigdomenech I, Ambrosi J-P, Eisenlohr L, Lartigue J E, Banwart S A, Bateman K, Milodowski A E, West J M, Griffault L, Gustafsson E, Hama K, Yoshida H, Kotelnikova S, Pedersen K, Michaud V, Trotignon L, Rivas Perez J, Tullborg E-L, 2001. O_2 depletion in granitic media. The REX project. SKB TR-01-05. Svensk Kärnbränslehantering AB.

Pusch R, Karnland O, 1990. Preliminary report on longevity of montmorillonite clay under repository-related conditions, SKB TR-90-44. Svensk Kärnbränslehantering AB.

Pusch R, 1999. Mobility and survival of sulphate-reducing bacteria in compacted and fully water saturated bentonite – microstructural aspects. SKB TR-99-30. Svensk Kärnbränslehantering AB.

Rich C I, 1968. Hydroxy interlayers in expansible layer silicates. Clays and Clay Minerals 16, 15–30.

Rivas Perez J, Banwart S A, Puigdomenech I, 2005. The kinetics of O_2(aq) reduction by structural ferrous iron in naturally occurring silicate minerals. Appl. Geochem. 20, 2003–2016.

Shen S, Stucki J W, Boast C W, 1992. Effects of structural iron reduction on the hydraulic conductivity of Na-smectite. Clays and Clay Minerals 40, 381–386.

SKB, 2006a. Long-term safety for KBS-3 repositories at Forsmark and Laxemar – a first evaluation. Main Report of the SR-Can project. SKB TR-06-09. Svensk Kärnbränslehantering AB.

SKB, 2006b. Buffer and backfill process report for the safety assessment SR-Can. SKB TR-06-18. Svensk Kärnbränslehantering AB.

Smart N R, Blackwood D J, Werme, L. 2001. The anaerobic corrosion of carbon steel and cast iron in artificial groundwaters. SKB TR-01-22. Svensk Kärnbränslehantering AB.

Smart N R, Rance A P, Werme L O, 2004. Anaerobic corrosion of steel in bentonite. Mat. Res. Soc. Symp. Proc. 807, 441–446.

Smith P, Johnson L, Snellman M, Pastina B, Gribi P, 2007. Safety assessment for a KBS-3H spent nuclear fuel repository at Olkiluoto – Evolution report. Posiva Report 2007-08 and SKB R-08-37. Posiva Oy, Olkiluoto, Finland. Svensk Kärnbränslehantering AB.

Steefel C I, 2006. CrunchFlow. Software for modeling multicomponent reactive flow and transport. User's manual. Lawrence Berkeley National Laboratories Report, Berkeley, USA.

Stroes-Gascoyne S, Hamon C J, Dixon D A, 2006. The effects of dry density and porewater salinity on the physical and microbiological characteristics of highly compacted bentonite. Ontario Power Generation Report No. 06819-REP-01200-10016-R00.

Stucki J W, Golden D C, Roth C B, 1984a. Effects of reduction and reoxidation of structural iron on the surface charge and dissolution of dioctahedral smectites. Clays and Clay Minerals 32, 350–356.

Stucki J W, Low P F, Roth C B, Golden D C, 1984b. Effects of oxidation state of octahedral iron on clay swelling. Clays and Clay Minerals 32, 357–362.

Stucki J W, Wu J, Gan H, Komadel P, Banin A, 2000. Effects of iron oxidation state and organic cations on dioctahedral smectite hydration. Clays and Clay Minerals 48, 290–298.

Tardy Y, Duplay J, 1992. A new method of estimating Gibbs energies of formation of hydrated and dehydrated clay minerals. Geochim. Cosmochim. Acta 56, 3007–3029.

Tomeoka K, McSween H Y, Buseck P R, 1989. Mineralogical alteration of CM carboneceous chondrites: a review. In: Hoshiai T. (ed.) Proceedings of the NIPR Symposium on Antarctic Meteorites, National Institute of Polar Research, Tokyo, 2, pp. 221–234.

Tournassat C, 2003. Cations-clays interactions: the Fe(II) case. Application to the problematic of the French deep nuclear repository field concept. PhD thesis, University of Grenoble, France, 199 p.

Viellard P, 2000. A new method for the prediction of Gibbs free energies of formation of hydrated clay minerals based on the electronegativity scale. Geochim. Cosmochim. Acta 48, 459–473.

Vieno T, 2000. Groundwater salinity at Olkiluoto and its effects on a spent fuel repository. Posiva Report 2000-11. Posiva Oy, Olkiluoto, Finland.

Vieno T, Lehikoinen J, Löfman J, Nordman H, Mészáros F, 2003. Assessment of disturbances caused by construction and operation of ONKALO. POSIVA 2003-06. Posiva Oy, Olkiluoto, Finland.

Vogt K, Köster H M, 1978. Zur Mineralogie, Kristallchemie und Geochemie einiger Montmorillonite aus Bentoniten. Clay Minerals 13, 25–43.

Wanner H, Wersin P, Sierro N, 1992. Thermodynamic modelling of bentonite-groundwater interaction and implications for near field chemistry in a repository for spent fuel. SKB TR-92-37. Svensk Kärnbränslehantering AB.

Wanner H, Albinsson Y, Karnland O, Wieland E, Wersin P, Charlet L, 1994. The acid/base chemistry of montmorillonite. Radiochim. Acta 66/67, 157–162.

Wersin P, Spahiu K, Bruno J, 1994. Time evolution of dissolved oxygen and repository conditions in a HLW repository. SKB TR-94-02. Svensk Kärnbränslehantering AB.

Wersin P, 2003. Geochemical modelling of bentonite porewater in high-level waste repositories. J. Contam. Hydrol. 61, 405–422.

Wersin P, Johnson L H, Schwyn B, Berner U, Curti E, 2003. Redox conditions in the near field of a repository for SF/HLW and ILW in Opalinus Clay. Nagra Technical Report NTB 02-13. Nagra, Wettingen, Switzerland.

Wersin P, Johnson L H, McKinley I G, 2007. Performance of the bentonite barrier beyond 100 C: a critical review. Physics and Chemistry of the Earth 32, 780–788.

Wilson J, Cressey G, Cressey B, Cuadros J, Ragnarsdottir K V, Savage D, Shibata M, 2006a. The effect of iron on montmorillonite stability: (II) Experimental investigation. Geochim. Cosmochim. Acta 70, 323–336.

Wilson J, Savage D, Cuadros J, Shibata M, Ragnarsdottir K V, 2006b. The effect of iron on montmorillonite stability. (I) Background and thermodynamic considerations. Geochim. Cosmochim. Acta 70, 306–322.

Xia X, Idemitsu K, Arima T, Inagaki Y, Ishidera T, Kurosawa S, Iijima K, Sato H, 2005. Corrosion of carbon steel in compacted bentonite and its effect on neptunium diffusion under reducing condition. Applied Clay Science 28, 89–100.

Yu J-W, Neretnieks I, 1997. Diffusion and sorption properties of radionuclides in compacted bentonite. SKB TR 97-12. Svensk Kärnbränslehantering AB.

Zolensky M H Y, McSween J R, 1988. Aqueous alteration. In Meteorites and the Early Solar System (eds. J.F. Kerridge and M.S. Matthews), University of Arizona Press, Tucson, pp. 114–143.

Appendix A

Input parameters for calculations

Values based on Johnson et al. (2005)

Parameter	Unit	Reference value
Drift per unit canister, diameter	mm	1,850
Drift per unit canister, length	mm	5,546
Drift per unit canister, volume	m^3	14.9078
Canister diameter	mm	1,050
Canister length	mm	4,830
Canister volume	m^3	4.1823
Supercontainer length	mm	5,546
Supercontainer inner diameter	mm	1,749
Supercontainer outer diameter	mm	1,765
Supercontainer thickness	mm	8
Supercontainer perforation degree	%	60
Supercontainer volume	m^3	0.0980
Supercontainer mass	kg	869
Bentonite final wet density	kg/m^3	2,000
Bentonite final dry density	kg/m^3	1,560
Bentonite final porosity	%	44
Bentonite final volume	m^3	10.3388
Bentonite final mass	kg	16,129